Mineralium Deposita
https://doi.org/10.1007/s00126-022-01133-z

ARTICLE

Multi-source and multi-stage metal mobilization during the tectonic evolution of the Central Lapland Greenstone Belt, Finland: implications for the formation of orogenic Au deposits

C. G. C. Patten[1] · F. Molnár[2,3] · I. K. Pitcairn[4] · J. Kolb[1] · S. Mertanen[2] · S. Hector[1]

Received: 7 August 2021 / Accepted: 26 July 2022

Abstract
Precambrian greenstone belts are prospective terrains for orogenic Au deposits worldwide, but the sources of Au, base metals, metalloids, and ligands enriched within the deposits are still debated. Metamorphic devolatilization is a key mechanism for generating Au-rich hydrothermal fluids, but the respective role of the metavolcanic and metasedimentary rocks present within these belts in releasing ore-forming elements is still not fully understood. The Central Lapland Greenstone Belt (CLGB), Finland, one of the largest Paleoproterozoic greenstone belts, hosts numerous orogenic Au deposits and is composed of variably metamorphosed volcanic and sedimentary rocks. Characterization of element behavior during prograde metamorphism highlights that (1) metavolcanic rocks release significant Au, As, Sn, Te, and possibly S; (2) metasedimentary rocks release significant S, C, Cu, As, Se, Mo, Sn, Sb, Te, and U, but limited Au; and (3) metakomatiite releases C and possibly Au. Throughout the CLGB metamorphic evolution, two main stages are identified for metal mobilization: (1) prograde metamorphism at ~ 1.92–1.86 Ga, promoting the formation of typical orogenic Au deposits and (2) late orogenic evolution between ~ 1.83 and 1.76 Ga, promoting the formation of both typical and atypical orogenic Au deposits. The complex lithologic diversity, tectonic evolution, and metamorphic history of the CLGB highlight that metal mobilization can occur at different stages of an orogenic cycle and from different sources, stressing the necessity to consider the complete dynamic and long-lasting evolution of orogenic belts when investigating the source of Au, ligands, metals, and metalloids in orogenic Au deposits.

Keywords Orogenic Au deposits · Metamorphic devolatilization · Metal mobilization · Metavolcanic rocks · Metasedimentary rocks

Introduction

Orogenic Au deposits are structurally controlled hydrothermal ore deposits that form in orogenic belts and account for a significant portion of the present and past global Au production (~ 30%; Frimmel 2018). These deposits are the product of complex large-scale processes, which include the production of metal-rich fluids, the transport of these fluids through the Earth's crust, and the precipitation of metals in structurally controlled locations at various degrees of metamorphism (Groves 1993, 1998; Pitcairn et al. 2006a; Large et al. 2011; Goldfarb and Groves 2015; Kolb et al. 2015). Production of metal-rich fluids is of paramount importance in the formation of any hydrothermal ore deposit (e.g., Fyfe 1987). Recognition of geological formations as sources of metals, ligands, and ore forming fluids is an important step for the investigation of metal-rich hydrothermal

Editorial handling: H. E. Frimmel

✉ C. G. C. Patten
clifford.patten@kit.edu

[1] Institute of Applied Geosciences, Chair of Geochemistry and Economic Geology, Karlsruhe Institute of Technology, 76131 Karlsruhe, Germany

[2] Geological Survey of Finland, P.O. Box 96, FI-02151 Espoo, Finland

[3] Institute of Geography and Earth Sciences, Budapest University, 1117 Budapest, Hungary

[4] Department of Geological Sciences, Stockholm University, SE-106 91 Stockholm, Sweden

Journal : Large 126	Article No : 1133	Pages : 28	MS Code : 1133	Dispatch : 10-9-2022

fluid genesis and ultimately for hydrothermal ore deposit formation. Although the mechanisms responsible for Au precipitation from hydrothermal fluids and the formation of orogenic Au deposits are fairly well constrained (Groves 1993; Groves et al. 1998; McCuaig and Kerrich 1998; Goldfarb and Groves 2015; Gaboury 2019), the sources of the metals, ligands, and fluids as well as the mineral reactions leading to the formation of Au-rich hydrothermal fluids are still debated (Goldfarb and Groves 2015; Groves et al. 2019). Three main sources have been proposed to generate metal-rich fluids in orogenic gold systems: (1) metamorphic devolatilization of supracrustal rocks (Fyfe 1987; Groves and Phillips 1987; Wyman and Kerrich 1988; Phillips and Powell 2010; Tomkins 2010), (2) subcontinental lithospheric mantle (Groves et al. 2019), and (3) magmatic sources (Burrows et al. 1986; Thébaud et al. 2018; Masurel et al. 2019).

In Precambrian greenstone belts hosting orogenic Au deposits, the source of metals and ligands is particularly cryptic (Goldfarb and Groves 2015; Groves et al. 2019), although metamorphic devolatilization appears to be a key process (Beaudoin and Chiaradia 2016; Patten et al. 2020; Pitcairn et al. 2021). Greenstone belts are dominated by metavolcanic rocks (basalt to rhyolite) with varying proportions of metasedimentary rocks and metakomatiite (de Wit and Ashwal 1995). The respective role of each lithology during metamorphic devolatilization in supplying metals, ligands, and/or hydrothermal fluids during dynamic and long-lasting orogenic evolution still remains poorly constrained. Metamorphic devolatilization of metasedimentary rocks is an efficient mechanism for generating metamorphic fluids enriched in S, As, and Au, the most common elements found in orogenic Au deposits (e.g., Boyle 1966; Pitcairn et al. 2006a, 2021; Tomkins 2010; Large et al. 2011; Goldfarb and Groves 2015). The scarcity of metasedimentary rocks relative to metavolcanic rocks in greenstone belts, however, implies that they cannot solely account for the formation of orogenic Au deposits (Goldfarb and Groves 2015). Metavolcanic rocks in greenstone belts, conversely, have long been suggested as potential source for metals (Phillips et al. 1987; Hronsky et al. 2012; Goldfarb and Groves 2015; Augustin and Gaboury 2017), and although they can release enough Au to account for orogenic gold endowment (Pitcairn et al. 2015; Patten et al. 2020), their capacity in releasing S, As, and other metals remains controversial (Goldfarb and Groves 2015; Pitcairn et al. 2015; Groves et al. 2019).

The Central Lapland Greenstone Belt (CLGB) in northern Finland is one of the largest known Paleoproterozoic greenstone belts (Hanski and Huhma 2005) and is an excellent target to study the source of metals in Precambrian orogenic Au deposits. The CLGB consists of a Paleoproterozoic sequence of oceanic crustal rocks and marine sedimentary rocks. The northern part of the CLGB is dominated by two main volcano-sedimentary sequences: the Kittilä and the Savukoski groups (Fig. 1). The Kittilä Group is dominated by tholeiitic metavolcanic rocks interbedded with various metasedimentary units (Hanski and Huhma 2005). The Savukoski Group is characterized by komatiitic and picritic metavolcanic rocks, which overlay pelitic metasedimentary rocks (Hanski and Huhma 2005). The CLGB displays a complex metamorphic pattern defined by zonation where the central area of the belt is metamorphosed at greenschist facies, whereas the margins are metamorphosed at amphibolite or granulite facies (Hölttä et al. 2007; Hölttä and Heilimo 2017).

The CLGB hosts numerous orogenic Au deposits, such as the 302 t Au Suurikuusikko deposit, but is relatively unexplored compared to other Paleoproterozoic greenstone belts (Mineral Deposit Database of Finland 2022; Niiranen et al. 2015). The orogenic Au deposits are preferentially located along the Kiistala shear zone (KiSZ) and the Sirkka shear zone (SiSZ), and are characterized by typical (Au-only) and atypical (Au-Cu-Co–Ni) metal associations (Eilu et al. 2007; Eilu 2015). Apart of a few occurrences in the marginal zones of the CLGB, most of the Au deposits occur in comparable lithological and structural settings characterized by greenschist facies metamorphism and have formed under similar physico-chemical conditions (Eilu et al. 2007; Eilu 2015). This suggests that the differences in the composition of the various deposits are, to some extent, controlled by the geochemical peculiarities of the source rocks.

In this study, we investigate the extent to which lithological units present in a greenstone belt contribute to the generation of metal-rich metamorphic fluids during metamorphic devolatilization. The outcomes show that combined metamorphic devolatilization of metavolcanic and metasedimentary rocks release sufficient metals and ligands to account for most of the Au and other metal endowments in orogenic Au deposits.

Tectonic setting

The Central Lapland Greenstone Belt

The CLGB is located in northern Finland and is exposed over an area of ≈ 20,000 km^2 (Fig. 1). It rests on the Archean (3.1–2.6 Ga) Karelian Craton. The volcano-sedimentary sequence records a complex geological evolution spanning from 2.45 to 1.76 Ga, including the 1.92–1.80 Ga Svecofennian orogeny (Hanski et al. 2001a; Hanski and Huhma 2005; Nironen 2017; Sayab et al. 2019). The CLGB is bound in the northeast by the Lapland Granulite Complex and to the south by the

Journal : Large 126 | Article No : 1133 | Pages : 28 | MS Code : 1133 | Dispatch : 10-9-2022

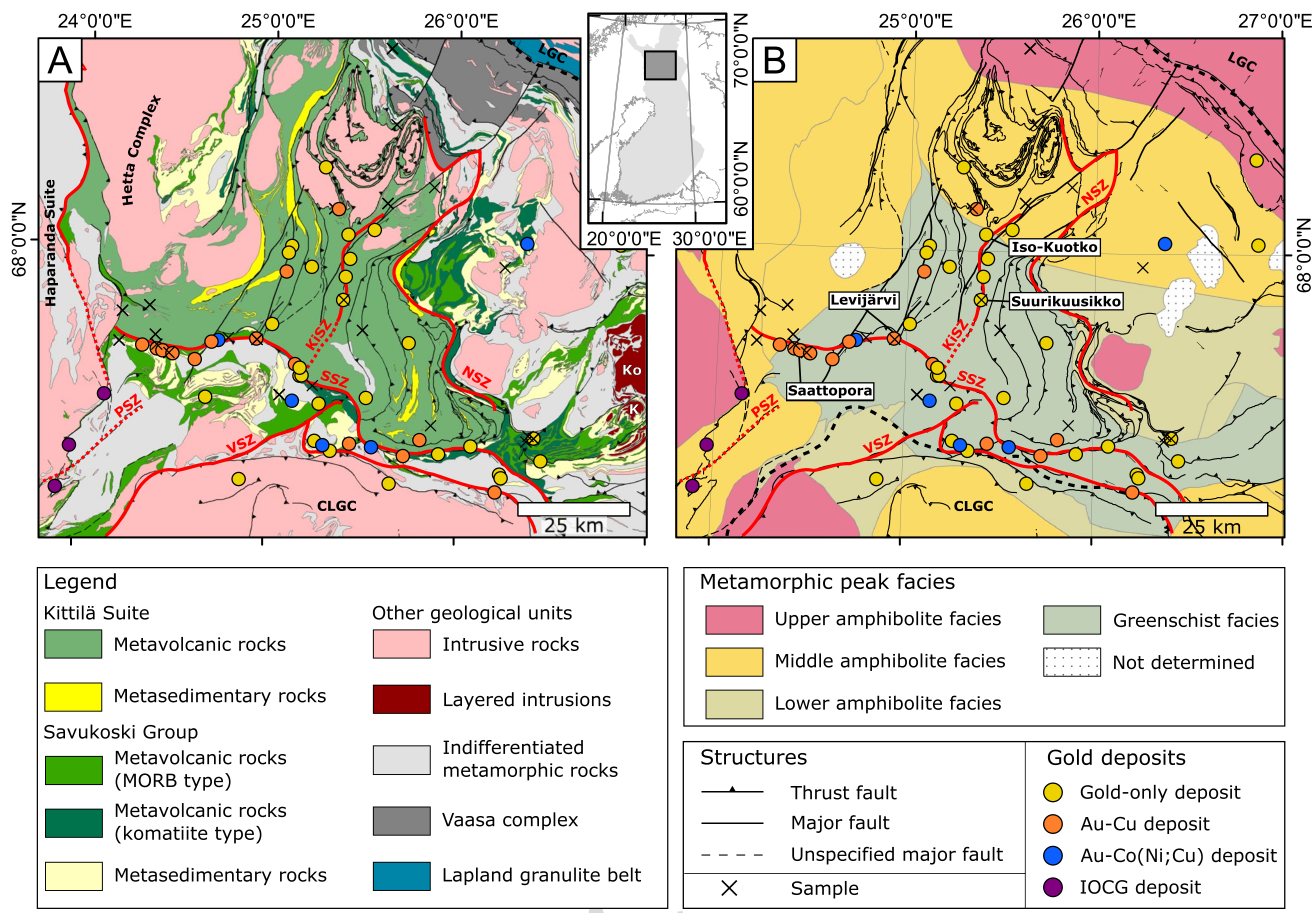

Fig. 1 Regional geological (**A**) and metamorphic map of the CLGB (**B**) showing major lithological units and orogenic Au deposits and showing major fault zones (KiSZ = Kiistala Shear Zone, SiSZ = Sirkka Shear Zone, PSZ: Pajala Shear Zone; VSZ: Venejoki Shear Zone, ESZ: Enontekiö Shear Zone; NSZ = Nolppio Shear Zone) complexes (CLGC = Central Lapland Granitoid Complex, LGC = Lapland Granulite Complex), intrusions (Ko: Koitelainen layered intrusion, K: Kevitsa layered intrusion), and sampled drillcore locations (black crosses). Simplified from the digital database of the Geological Survey of Finland

Central Lapland Granitoid Complex (Fig. 1). The Pajala Shear Zone separates the CLGB from the Norrbotten structural domain in the west. To the east and southeast, the CLG is bound by the Nolppio Thrust and Nolppio Shear Zone.

The CLGB is divided into six main lithostratigraphic units from the base to the top of the lithostratigraphy: the Salla, Onkamo (or Kuusamo), Sodankylä, Savukoski, Kittilä, Laino, and Kumpu groups. The Salla and Onkamo groups are dominated by intermediate to felsic metavolcanic rocks and metakomatiite, respectively. They formed during rifting of the Archean basement at ca. 2.45–2.2 Ga (Hanski and Huhma 2005; Hanski et al. 2001a). At ca. 2.45 Ga, several layered igneous complexes (e.g., Koitelainen layered intrusion) were emplaced in the Salla Group but not the Onkamo Group. The Sodankylä Group is characterized by continental metasedimentary rocks, such as quartzite and mica schist. They correspond to a long depositional period before 2.2 Ga, the age of mafic dikes cutting this unit (Hanski et al. 2001a; Hanski and Huhma 2005). The Sodankylä Group metasedimentary rocks grade transgressively into the deeper-water pelitic sedimentary rocks of the Savukoski Group (Hanski and Huhma 2005). The Savukoski Group metasedimentary rocks are overlain by komatiitic and picritic-dominated metavolcanic rocks with 2.05 Ga minimum age corresponding to the age of the Kevitsa-layered intrusion (Hanski and Huhma 2005; Hanski et al. 2001a). Some of the volcanic rocks in the Kittilä Group are probably parautochthonous, and some consist of 2.01 Ga allochthonous tholeiitic metavolcanic rocks representative of an ancient oceanic lithosphere (Hanski and Huhma 2005). It is subdivided into four formations: (1) the Kautileskä Formation, dominated by metavolcanic rocks with within plate basalt (WPB) affinity and minor metasedimentary rocks such as phyllite, black schist, metagraywacke, and metacarbonate rocks; (2) the Porkonen Formation, dominated by banded iron formation; (3) the Vesmajärvi Formation, dominated by metavolcanic rocks with mid-oceanic ridge basalt (MORB) affinity; and (4) the Pyhäjärvi Formation, dominated by micaschist and metagreywacke (Lehtonen et al. 1998; Hanski and Huhma 2005). At 1.92 Ga, the Kittilä Group has been thrust onto the Savukoski Group (Hanski and Huhma 2005). Finally, the Laino and Kumpu groups cap unconformably the previous groups and are characterized by molasse-type sediments of ca. 1.88 Ga maximum age (Hanski and Huhma 2005; Hanski et al. 2001a; Hölttä et al. 2007).

Deformation and metamorphism of the CLGB

The CLGB is characterized by a complex tectonic evolution defined by different deformation and metamorphic events in space and time. Following Archean basement extension, deformation occurred at ca. 1.93–1.91 Ga with east–west bulk shortening (D1) as the result of the collision between the Norrbotten and Karelia blocks and development of a foreland fold-and-thrust-belt (Hanski and Huhma 2005; Nironen 2017; Sayab et al. 2019). Tectonic juxtaposition of the Kittilä Group onto the Savukoski Group led to formation of moderately dipping thrust zones within and at the base of the Kittilä Group, such as the KiSZ (Hanski and Huhma 2005; Nironen 2017; Sayab et al. 2019). Shortly after D1, the collision between the Karelia and Lapland-Kola blocks at ca. 1.90–1.89 Ga led to north–south shortening (D2) and thrusting of the Lapland Granulite Belt onto the CLGB from the northeast. To the south, D2 led to a new east–west orientated thrust system with the development of the SiSZ and leading to the thrusting of the Savukoski Group onto the Kittilä Group. The KiSZ, truncated by the SiSZ in the south, acted as transfer fault (Hanski and Huhma 2005; Nironen 2017; Sayab et al. 2019). Progressive clockwise rotation into northeast-vergent compression occurred at ca. 1.88–1.87 Ga (D3), switching the deformation regime from compressional to transpressional and leading to dextral strike-slip in the KiSZ (Hanski and Huhma 2005; Nironen 2017; Sayab et al. 2019). A nearly 90° switch in the regional stress field occurred at ca. 1.84–1.81 Ga leading to a northwest-southeast compressional regime (D4). The D4 led to flipping of the kinematics in the KiSZ from dextral to sinistral strike-slip and to reactivation of the SiSZ (Nironen 2017; Sayab et al. 2019). Orogenic collapse occurred during 1.80–1.77 Ga with NE-SW extension and granite emplacement (Hanski and Huhma 2005; Nironen 2017). At ca. 1.77–1.76 Ga, east–west shortening (D5) led to localized fault reactivation (Nironen 2017; Sayab et al. 2019).

In the CLGB, the Paleoproterozoic volcanic-sedimentary sequence was affected by several metamorphic events, the intensity and timing of which did not occur homogeneously throughout the belt, leading to a complex metamorphic pattern. In the central part of the CLGB, peak metamorphism is inferred at ca. ~ 1.88–1.86 Ga during D2–D3 and reached greenschist-facies conditions at 250–400 °C, the lowest metamorphic grade of the belt (Fig. 1; Hölttä et al. 2007; Hölttä and Heilimo 2017; Nironen 2017; Molnár et al. 2018). Metavolcanic and metasedimentary rocks generally preserved their primary magmatic and sedimentary textures (Hölttä et al. 2007). Age of metamorphism in the external part of the belt is less well constrained. Progressive thrusting of the Lapland Granulite Belt during D2–D3 onto the CLGB from the northeast led to inverted metamorphic gradients in the northeastern part of the latter (Hölttä et al. 2007; Hölttä and Heilimo 2017). Granulite-facies metamorphism (770–890 °C) was initiated at ca. 1.89 Ga at the margin of the Lapland Granulite Belt and propagated towards the southwest into the CLGB until ~ 1.82 Ga, leading to amphibolite-facies metamorphism (Fig. 1; Hölttä and Heilimo 2017; Nironen 2017). In the western part of the CLGB, thrusting towards the east of the Haparanda Suite along the Enontekiö Shear Zone, at ca. 1.86–1.85 Ga, led as well to inverted metamorphic gradient up to mid-amphibolite facies (Bergman et al. 2006; Nironen 2017). Additionally, thrusting during D3–D4 from the south resulted in emplacement of amphibolite-facies metamorphic rocks from the Central Lapland Granitoid Complex onto the Savukoski Group in the southern part of the CLGB along the Venejoki Shear Zone (Fig. 1; Bergman et al. 2006; Hölttä et al. 2007; Hölttä and Heilimo 2017; Nironen 2017; Lahtinen et al. 2018). The resulting effect from thrusting of the Lapland Granulite Belt from the north-northeast, the Haparanda Suite from the west, and the Central Lapland Complex from the south explains the specific concentric metamorphic pattern of the CLGB with greenschist facies in the center and increasing metamorphic grade outwards (Fig. 1). These complex and long-lasting thrusting events on the margins of the CLGB most likely led to different ages of peak metamorphism for the lithological units of the CLGB. These are most likely related to D2–D3, but a more detailed constraint on these ages is not currently available (Hölttä et al. 2007; Hölttä and Heilimo 2017; Nironen 2017; Sayab et al. 2019). A late metamorphic event throughout the belt at around ~ 1.80–1.78 Ga and related to D4–D5 is outlined by U–Pb ages of metamorphic titanites and monazite, possibly related to orogenic collapse (Rastas et al. 2001; Hölttä et al. 2020). Finally, concomitantly to metamorphism, several crustal melting events produced orogenic granitoids at ~ 1.88–1.87 Ga and ~ 1.81–1.77 Ga throughout the CLGB (Fig. 1; Ahtonen et al. 2007; Lahtinen et al. 2018).

Journal : Large 126	Article No : 1133	Pages : 28	MS Code : 1133	Dispatch : 10-9-2022

Table 1 Main typical and atypical orogenic Au deposits of the CLGB

Deposit	Deposit type	Structural control	Ore assemblage	Age	Deformation stage	Gold occurrence	References
Suurikuusikko	Typical Au-only	KiSZ	Py, Apy	1.92 Ga	D1	Refractory	Patison (2007), Wyche et al. (2015), Molnár et al. (2018), Sayab et al. (2019)
Iso-Kuotko	Typical Au-only	KiSZ	Apy, Py, Po, Cpy, Gn	1.87–1.86 Ga; main event at 1.77–1.76 Ga	D5	Native and refractory	Molnár et al. (2018), Sayab et al. (2019)
Levijärvi-Loukinen	Atypical Au-Cu-Ni-Co	SiSZ	Po, Cpy, Py, Ger, Aspy	1.90–1.76 Ga; main event at 1.8–1.76 Ga	D2–D5	Native and inclusions	Molnár et al. (2017), Kurhila et al. (2017), Holma and Keinanen (2007), Patison (2007), Nironen (2017), Sayab et al. (2019)
Saattopora	Atypical Au-Cu	SiSZ	Po, Cpy, Pn, Ger, Cob, Aspy	1.87–1.79 Ga; main event at 1.82–1.79 Ga	D4	Native and inclusions	Molnár et al. (2019), Patison (2007); Nironen (2017), Sayab et al. (2019)

Py pyrite, *Apy* arsenopyrite, *Po* pyrrhotite, *Cpy* chalcopyrite, *Gn* galena, *Pn* pentlandite, *Cob* cobaltite, *Ger* gesdorffite

Gold endowment in the CLGB

Orogenic Au deposits in the CLGB are spatially controlled by the KiSZ and SiSZ (Fig. 1; Patison 2007). The typical orogenic Au deposits are best represented by the Suurikuusikko deposit (Kittilä mine), the largest Au mine in Europe with ~ 302 t Au reserves, and the Iso-Kuotko deposit, 12 km north of the Suurikuusikko deposit along the KiSZ (Fig. 1; Table 1; Mineral Deposit Database of Finland 2022). The atypical orogenic Au deposits, on the other hand, are best represented by the Au-Cu Saattopora and the Au-Cu-Ni-Co Levijärvi-Loukinen deposits, located in the western and central part of the SiSZ, respectively (Fig. 1; Table 1; Holma and Keinanen 2007; Kurhila et al. 2017; Molnár et al. 2017).

The typical and atypical orogenic Au deposits in the CLGB share many characteristics. They show strong structural control, and the orebodies generally occur as swarms of elongated lodes (Eilu et al. 2007; Eilu 2015). Differences in rheological properties of rock types present, such as ultramafic and metasedimentary rocks, have important control on the mineralization, especially when competency is enhanced by early albite alteration promoting brittle behavior (Eilu et al. 2007; Patison 2007; Eilu 2015). Most of the deposits formed under similar temperature and pressure conditions, at 250–450 °C and 1–3 kbar, respectively, and the ores typically contain 1–5% sulfide with gold being either free, as inclusions or refractory (Eilu et al. 2007; Eilu 2015; Sayab et al. 2016). Despite the similarities, the typical and atypical orogenic Au deposits also show important differences. The typical orogenic Au deposits are generally dominated by pyrite, pyrrhotite, and arsenopyrite whereas the atypical ones show greater mineralogical diversity with pyrite, pyrrhotite, arsenopyrite, chalcopyrite, cobaltite, pentlandite, and gersdorffite, reflecting differences in metal endowment (Table 1; Eilu 2015). The typical orogenic Au deposits are preferentially located along the KiSZ whereas the atypical ones are located along the SiSZ (Fig. 1). Geochronological studies indicate that orogenic Au mineralization in the CLGB occurred during the D1–D3 events, at ~ 1.92–1.86 Ga, and later during the D4–D5 events at ~ 1.81–1.76 Ga (Wyche et al. 2015; Molnár et al. 2018; Sayab et al. 2019). The first Au mineralization stage in the CLGB, occurring as early as 1.92 Ga and apparently pre-dating peak metamorphism at the Suurikuusikko deposit (Wyche et al. 2015; Molnár et al. 2018), appears to be best recorded along the KiSZ whereas the second Au mineralization stage is recorded along both the KiSZ and SiSZ (e.g., Iso-Kuotko, Saattopora and Levijärvi-Loukinen; Table 1).

Journal : Large 126 | Article No : 1133 | Pages : 28 | MS Code : 1133 | Dispatch : 10-9-2022

Sampling and analytical method

A suite of 105 drill core samples from the Kittilä Group and Savukoski Group, distal from the hydrothermally altered zones surrounding gold deposits, were selected. They are representative of the variation in lithology and metamorphic facies within the CLGB (Fig. 1). They include 36 metavolcanic rocks and 17 metasedimentary rocks from the Kittilä Group and 25 metavolcanic and 27 metasedimentary rocks from the Savukoski Group (ESM 1). The metamorphic grade ranges from greenschist to upper amphibolite facies with greenschist-facies samples generally preserving their primary features such as pillow rims and vesicles in metavolcanic rocks, whereas upper amphibolite-facies samples are variably foliated, sheared, and deformed. Of the selected samples, 43 are metamorphosed to greenschist facies (300–400 °C), 35 to lower amphibolite facies (450–550 °C), and 29 to upper amphibolite facies (> 550 °C; Hölttä and Heilimo 2017).

Major and trace elements were analyzed for in two batches by ALS Minerals and Labtium. From the samples sent to ALS Mineral, major elements were analyzed for by XRF; Ba, Ce, Cr, Cs, Dy, Er, Eu, Ga, Cd, Ge, Hf, Ho, La, Lu, Nb, Nd, Pr, Rb, Sm, Sn, Sr, Ta, Tb, Th, Tm, U, V, W, Y, Yb, and Zr by ICP-MS from lithium borate fusion disks after acid digest; Ag, Cd, Co, Cu, Li, Mo, Ni, Pb, Sc, and Zn by ICP-AES after four acid digest (HNO_3, HF, $HClO_4$, HCl); As, Bi, Hg, In, Re, Sb, Sc, Se, Te, and Tl by ICP-MS after aqua regia acid digest; and S and C by LECO furnace. A suite of standards (GIOP-102 for XRF analysis; AMIS0304, GBM908-10, GBM908-5, and GEOMS-03 for ICP-MS analysis; GEOMS-03 for ICP-AES analysis; GGC-09, GS303-9, GS310-10, and GS910-4 for LECO furnace analysis), duplicated samples, and blanks were analyzed to check for accuracy, precision, and limits of detection (ESM 2). For the samples sent to Labtium, major elements were analyzed for by XRF on pressed pellets; Ce, Dy, Er, Eu, Gd, Hf, Ho, La, Lu, Nb, Nd, Pr, Rb, Sm, Ta, Tb, Th, Tm, U, Y, Yb, Ag, As, Be, Bi, Cd, Ce, Dy, Er, Eu, Gd, Hf, Ho, La, Lu, Mo, Nb, Nd, Pr, Rb, Sm, Ta, Tb, Lu, Nb, Nd, Pb, Pr, Rb, Sb, Se, Sm, Sn, Ta, Tb, Te, Th, Tm, U, W, Y, and Yb by ICP-MS after HF-$HClO_4$ and aqua regia digestion; Co, S, Sc, V, and Zr by ICP-AES after HF-$HClO_4$ digest; and C by C-analyzer. A suite of standards was analyzed to check for accuracy, precision, and limit of detections (ESM 2). Gold whole rock analyses were carried out at Stockholm University following the ultra-low detection limit technique developed by Pitcairn et al. (2006b). To minimize possible nugget effects, 3 g of sample powder was digested by HNO_3-HF-aqua regia into liquid solution. The solutions were analyzed using a Thermo Fisher XSeries 2 ICP-MS. The 3σ method detection limit calculated from blank digests is 0.027 ppb. Analytical accuracy and precision were controlled through analyses of CANMET reference material TDB-1 and USGS reference materials WMS-1 and CH-4, which have reproducibility of 104%, 91%, and 87%, respectively (Patten et al. 2020).

Rock classification

Metavolcanic rocks

The Kittilä and Savukoski groups contain several genetically unrelated metavolcanic rocks (Lehtonen et al. 1998; Hanski and Huhma 2005), and thus, metavolcanic rocks show significant variations in major and trace element concentrations (Table 2).

Kittilä Group

Samples from the Kittilä Group are MORB ($n = 13$), WPB ($n = 17$), and boninite-like dikes ($n = 6$; Fig. 2; Hanski and Huhma 2005). The MORB-like samples, which are part of the Vesmajärvi Formation (Lehtonen et al. 1998; Hanski and Huhma 2005), are dominantly basalt (45.2–53.0 wt% SiO_2) with tholeiitic to transitional affinity (Zr/Y < 3.75 and Th/Yb < 0.69; Fig. 2). Relatively flat REE profiles ($La/Yb_{pm} = 1.70 \pm 0.72$; Fig. 2) suggest an E-MORB affinity. The WPB-like samples, which are part of the Kautoleskä Formation (Lehtonen et al. 1998; Hanski and Huhma 2005), are also dominantly basaltic (46.0–51.6 wt% SiO_2), but have slightly higher $Na_2O + K_2O$ content than the MORB-like samples (3.93 ± 1.1 wt%), and three samples classify as trachy-basalt (Fig. 2). The WPB-like samples have a transitional to calc-alkaline affinity (Zr/Y > 4.61 and Th/Yb > 0.42; Fig. 2). The REE profiles show LREE enrichment relative to HREE ($La/Yb_{pm} = 5.91 \pm 2.75$; Fig. 2) and significant negative Ta and Nb anomalies relative to Th ($Ta/Th_{pm} = 0.69 \pm 0.36$ and $Nb/Th_{pm} = 0.76 \pm 0.45$). The boninite-like dikes are characterized by higher MgO (8.79 ± 0.28 wt%) and lower TiO_2 (0.51 ± 0.04 wt%; Table 1) than MORB and WPB and have a transitional affinity (1.7–3.09 Zr/Y and 0.41–0.52 Th/Yb; Fig. 2). Their REE profiles show slight LREE enrichment relative to HREE ($La/Yb_{pm} = 2.1 \pm 0.2$; Fig. 2) and slight negative Ta and Nb anomalies relative to Th ($Ta/Th_{pm} = 0.32 \pm 0.03$ and $Nb/Th_{pm} = 0.44 \pm 0.05$; Fig. 2).

Journal : Large 126 | Article No : 1133 | Pages : 28 | MS Code : 1133 | Dispatch : 10-9-2022

Table 2 Whole rock composition of the different lithologies present in the Kiitilä and Savukoski groups

		SiO_2	Al_2O_3	Fe_2O_3	MgO	CaO	Na_2O	K_2O	TiO_2	P_2O_5	MnO	Total	LOI	S	C	Co	Cu	As	Se	Mo	Sn	Sb	Te	Au	U
		wt%	wt%	wt%	wt%	wt%	wt%	wt%	wt%	wt%	wt%	wt%	wt%	wt%	wt%	ppm	ppm	ppm	ppm	ppm	ppm	ppm	ppm	ppb	ppm
Metavolcanic rocks from Kittilä Group and Savukoski Suite																									
MORB ($n=19$)	Mean	49.0	14.1	13.6	6.9	10.0	2.5	0.4	1.30	0.18	0.21	98.2	2.1	0.16	0.32	48.70	83.94	11.56	0.62	0.87	1.36	0.16	0.02	1.27	0.03
	σ	2.0	1.0	2.2	1.7	2.2	0.9	0.4	0.40	0.16	0.03	1.1	2.0	0.17	0.40	9.80	51.27	22.30	0.35	0.53	0.84	0.09	0.02	1.91	0.03
	Median	**48.8**	**14.2**	**13.2**	**7.2**	**10.3**	**2.5**	**0.3**	**1.24**	**0.11**	**0.21**	**98.4**	**1.4**	**0.14**	**0.16**	**48.86**	**90.30**	**1.25**	**0.51**	**1.01**	**1.04**	**0.13**	**0.02**	**0.65**	**0.02**
WPB ($n=21$)	Mean	49.2	13.7	13.7	6.3	9.1	3.2	0.8	1.82	0.27	0.22	98.3	2.0	0.13	0.38	47.68	85.22	11.31	0.61	0.89	4.08	0.20	0.02	1.78	0.04
	σ	2.6	1.6	2.2	1.7	2.2	0.9	0.6	0.54	0.11	0.05	1.2	1.7	0.15	0.34	12.71	58.87	19.12	0.27	0.58	9.53	0.21	0.01	2.83	0.04
	Median	**48.7**	**13.7**	**14.2**	**6.1**	**9.1**	**3.1**	**0.8**	**1.84**	**0.24**	**0.22**	**98.7**	**1.7**	**0.09**	**0.22**	**45.51**	**71.38**	**2.11**	**0.59**	**0.69**	**0.66**	**0.12**	**0.02**	**0.69**	**0.02**
Komatiite ($n=16$)	Mean	46.5	7.4	12.3	23.9	8.4	0.6	0.1	0.53	0.04	0.17	100.0	7.9	0.06	1.38	89.11	26.83	1.26	0.18	0.38	0.14	0.15	0.87	0.66	0.02
	σ	3.1	1.9	1.6	5.3	1.9	0.8	0.1	0.24	0.02	0.03	5.0	5.5	0.09	1.55	18.18	31.49	0.98	0.12	1.12	0.07	0.05	3.33	0.57	0.01
	Median	**47.1**	**7.1**	**12.2**	**24.8**	**8.3**	**0.4**	**0.1**	**0.48**	**0.04**	**0.17**	**101.0**	**7.1**	**0.01**	**0.47**	**93.47**	**12.14**	**0.90**	**0.14**	**0.09**	**0.11**	**0.13**	**0.01**	**0.43**	**0.01**
Boninite ($n=6$)	Mean	50.5	14.6	9.2	8.8	10.8	2.5	0.7	0.51	0.04	0.19	97.7	0.9	0.16	0.06	37.54	68.31	1.56	0.31	13.13	1.01	0.08	2.60	0.79	0.03
	σ	1.6	0.7	0.5	0.3	1.0	0.7	0.4	0.04	0.00	0.01	2.8	0.3	0.18	0.07	4.10	51.30	2.85	0.10	0.00	0.00	0.04	6.32	0.47	0.02
	Median	**51.1**	**14.9**	**9.2**	**8.8**	**10.5**	**2.8**	**0.8**	**0.51**	**0.04**	**0.19**	**98.8**	**1.0**	**0.07**	**0.04**	**36.82**	**73.68**	**0.40**	**0.30**	**13.13**	**1.01**	**0.08**	**0.03**	**0.72**	**0.03**
Metasedimentary rocks from Kittilä Group and Savukoski Suite																									
Volcano-clastic rocks ($n=13$)	Mean	53.2	15.0	15.5	4.6	3.1	2.5	1.9	1.7	0.17	0.20	97.9	1.74	0.14	0.30	49.0	60.0	24.2	0.58	0.72	1.40	0.24	0.02	1.39	1.13
	σ	4.9	2.0	2.7	1.9	2.6	1.2	1.2	0.6	0.13	0.09	1.60	1.09	0.13	0.26	9.4	66.3	27.2	0.25	0.89	0.36	0.01	0.31	1.58	0.93
	Median	**52.8**	**14.9**	**15.5**	**3.6**	**2.1**	**2.8**	**1.7**	**1.7**	**0.12**	**0.21**	**98.9**	**1.83**	**0.13**	**0.28**	**45.8**	**39.9**	**9.0**	**0.57**	**0.41**	**0.10**	**0.02**	**0.02**	**0.57**	**1.30**
S- and C-rich metasedi-mentary rocks ($n=31$)	Mean	50.2	13.0	17.1	4.8	5.7	1.7	2.6	1.4	0.31	0.20	96.98	7.17	4.46	2.90	81.1	345	82.4	6.85	16.90	5.12	0.21	0.08	1.86	7.80
	σ	8.0	3.9	8.1	2.8	4.3	1.7	1.5	0.7	0.39	0.20	2.03	3.76	5.26	2.60	122.2	421	169	10.59	23.16	14.99	0.31	0.01	5.38	9.62
	Median	**48.7**	**13.2**	**15.2**	**4.7**	**5.2**	**1.1**	**2.9**	**1.3**	**0.20**	**0.14**	**97.3**	**6.10**	**2.69**	**2.20**	**50.3**	**200**	**13.1**	**1.91**	**9.50**	**0.53**	**0.08**	**0.08**	**0.39**	**4.84**

Journal : Large 126 | Article No : 1133 | Pages : 28 | MS Code : 1133 | Dispatch : 10-9-2022

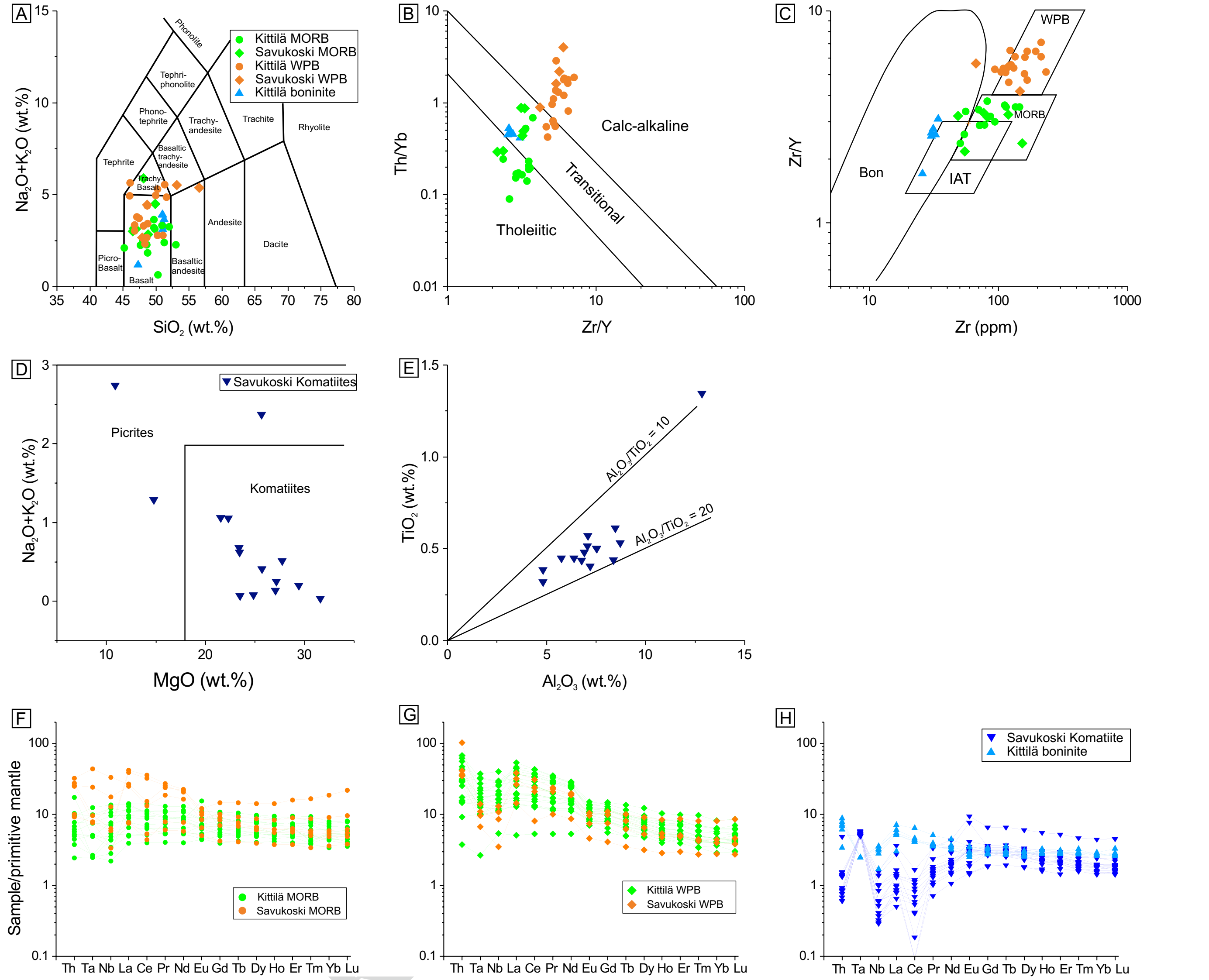

Fig. 2 Geochemical classification of the metavolcanic rocks (MORB, WPB, boninite-like dike and komatiite) from the Kittilä and Savukoski groups. **A** from Le Bas et al. (1986), **B** from Ross and Bédard (2009), **C** from Pearce and Norry (1979), **D** from Le Bas (2000), **E** from Barnes and Often (1990), and **F–H** primitive mantle values from McDonough and Sun (1995)

Savukoski Group

Samples from the Savukoski Group are mostly metakomatiite ($n = 15$) with minor MORB ($n = 6$) and WPB ($n = 4$) type metabasalt. Metakomatiite is characterized by 46.5 ± 3.1 wt% SiO_2 and 23.9 ± 5.3 wt% MgO (Table 2) and is Al-undepleted ($TiO_2/Al_2O_3 = 14.7 \pm 1.89$; Fig. 2; Barnes and Often 1990). Two samples have $Na_2O + K_2O > 2$ wt%, and two have MgO < 18 wt%, but these samples are classified nevertheless as metakomatiite based on their REE profiles (Fig. 2). The REE profiles are characterized by HREE enrichment relative to LREE ($La/Yb_{pm} = 0.66 \pm 0.31$; Fig. 2). The MORB-like samples are basaltic (47.8 ± 1.3 wt% SiO_2) with tholeiitic to transitional affinity (Zr/Y < 2.9 and Th/Yb < 0.55; Fig. 2). They show slightly enriched REE profiles ($La/Yb_{pm} = 3.9 \pm 3.1$; Fig. 2) suggesting an E-MORB affinity similarly to the Kittilä Group. Two samples have transitional Zr/Y and Th/Yb values and REE patterns similar to WPB. The WPB-like samples are basaltic to andesitic (51.6 ± 4.0 wt% SiO_2) with transitional to calc-alkaline affinity (Zr/Y > 4.2 and Th/Yb > 0.89; Fig. 2). The REE profiles are similar to the Kittilä Group with LREE enrichment relative to HREE ($La/Yb_{pm} = 6.2 \pm 2.1$; Fig. 2) and strong negative Ta and Nb anomalies relative to Th ($Ta/Th_{pm} = 0.22 \pm 0.10$ and $Nb/Th_{pm} = 0.20 \pm 0.12$).

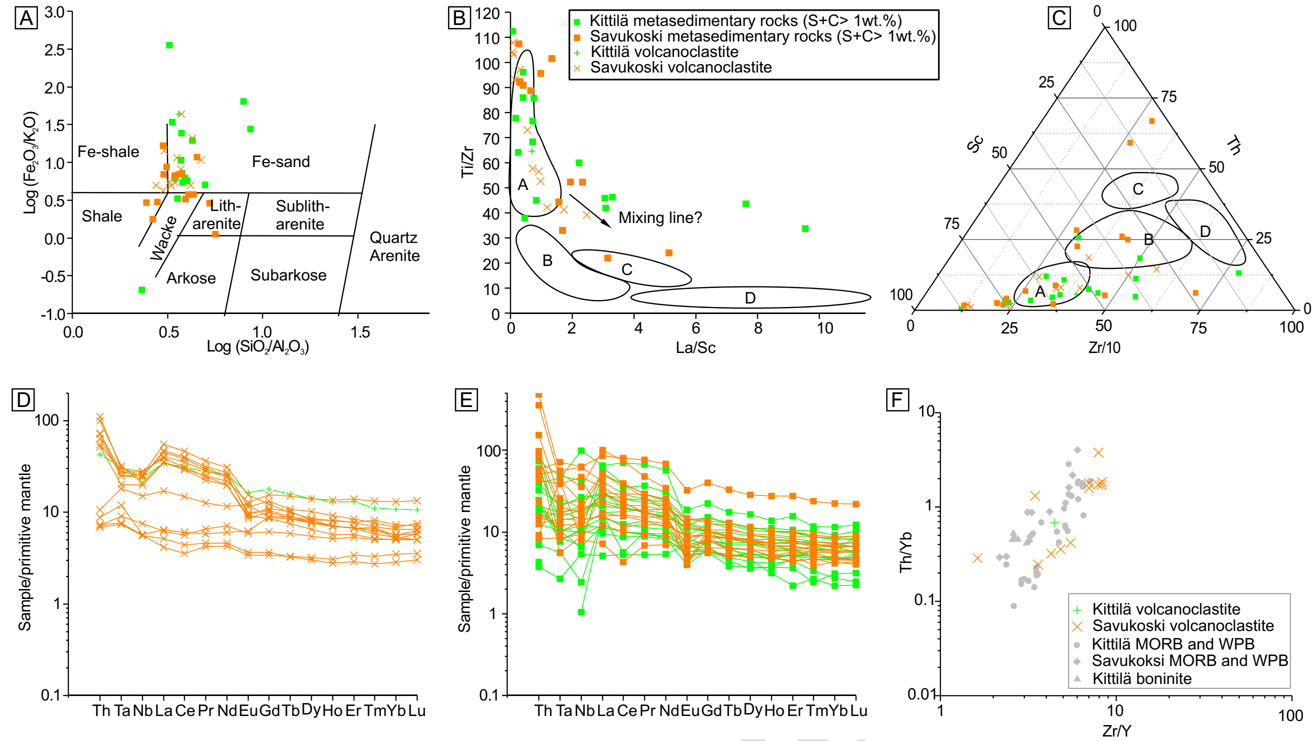

Fig. 3 Geochemical classification of the metasedimentary rocks from the Kittilä and the Savukoski groups. **A** From Herron (1988), **B**, **C** from Bhatia and Crook (1986), A = oceanic island arc, B = continental island arc, C = active continental arc, and D = passive margin, **D**, **E** primitive mantle values from McDonough and Sun (1995), and **F** from Ross and Bédard (2009)

Metasedimentary rocks

Kittilä Group

Metasedimentary rocks occur as intercalated units within the metavolcanic rocks. They comprise mainly metagraywacke, phyllite and black schist with variable sulfide and carbonaceous material contents (Hanski and Huhma 2005). Selected samples classify as wacke and Fe sand (Fig. 3) and show wide range in major and trace element concentrations (Table 2). Immobile trace element concentrations suggest an oceanic-arc dominated source (Fig. 3). These samples have a wide range of S and C contents ranging between 0.02–20.5 wt% S and 0.66–12.4 wt% C but with total S + C > 1 wt%. Samples with the highest S and C contents are black schists with sulfidic seams. One competent and poorly foliated sample with S + C < 1wt% has a composition similar to that of WPB-like samples (Fig. 3) suggesting that it represents a metamorphosed volcanoclastic rock.

Savukoski Group

Metasedimentary rocks are common and constitute the base of the group on top of which the metavolcanic rocks were conformably emplaced (Hanski and Huhma 2005). They mostly consist of phyllite, black schist, and mafic metatuffites (Hanski and Huhma 2005). Selected samples classify as Fe-shale, shale, wacke, and litharenite as protoliths (Fig. 3). Similar to rocks from the Kittilä Group, they show a wide range in major and trace element concentrations (Table 2). The immobile element concentration suggests either an active continental margin or an oceanic island arc source (Fig. 3). The S and C concentrations range between 0.01 and 11.04 wt% and 0.02 and 8.14 wt%, respectively, with black schists being the most S- and C-rich samples. Poorly foliated and competent samples with S + C < 1wt% are common ($n = 12$) and have similar composition to that of MORB and WPB samples, suggesting that they represent metamorphosed volcanoclastic rocks (Fig. 3).

Element distribution related to metamorphism

Metavolcanic and metavolcanoclastic rocks with MORB and WPB signatures

Due to similar geochemistry, metavolcanic and metavolcanoclastic rocks are grouped together when compared to

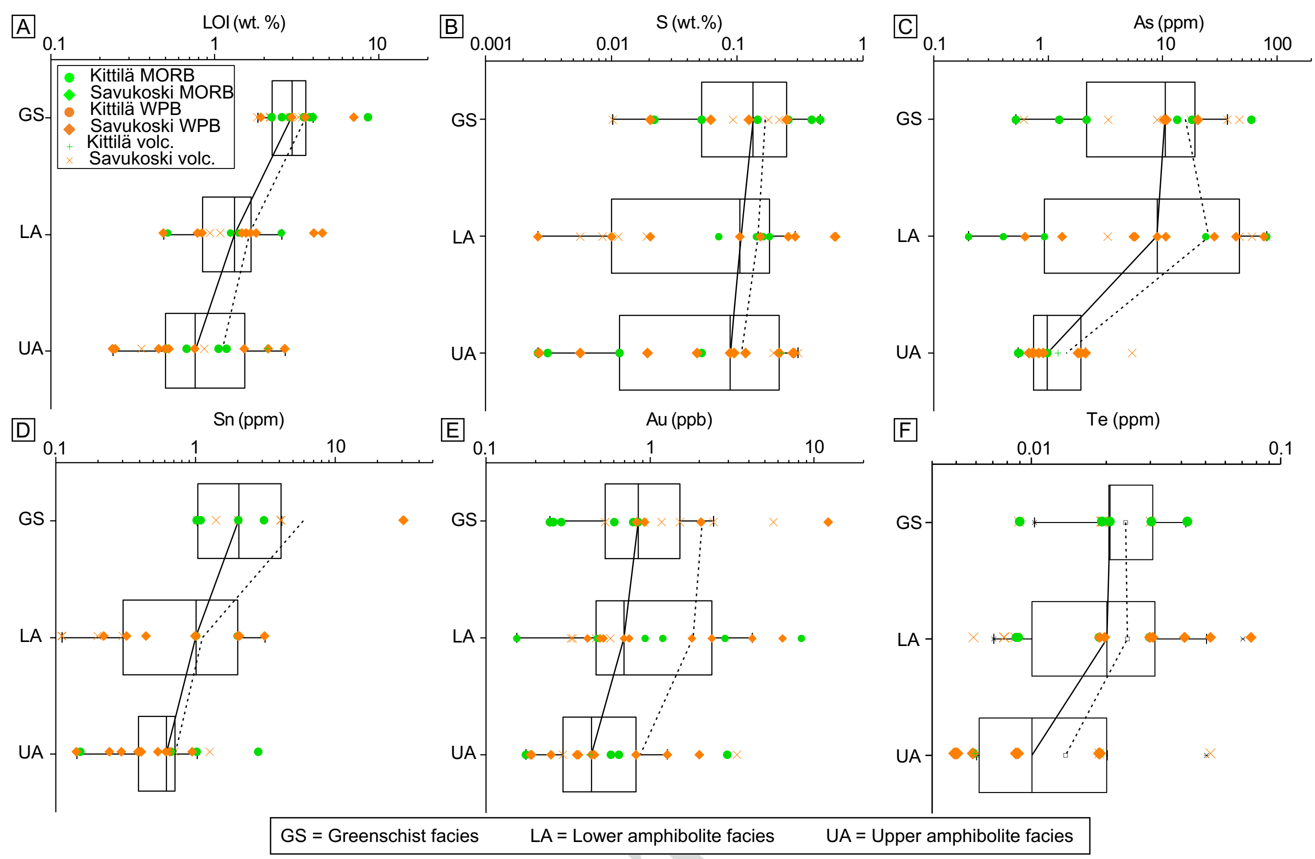

Fig. 4 **A** LOI, **B** S, **C** As, **D** Sn, **E** Au, and **F** Te content in metavolcanic and metavolcanoclastic rocks from Kittilä Group and Savukoski Group according to their metamorphic facies. Only elements showing systematic variation in composition with metamorphic grade are shown. Solid curve connects median values of each group, whereas dashed curve connects average values. The box ranges are defined by the 25th and 75th percentiles, and the whiskers by the lower and inner fence

metamorphic grade. Boninites, however, are not grouped with MORB and WPB as they are volumetrically minor, not well genetically characterized and geochemically different (Table 2). Differences in trace element distribution in MORB, WPB, and related metavolcanoclastic rocks are observed relative to metamorphism (Fig. 4). To describe variations in element concentration relative to metamorphism, median and box plots are used rather than the average and standard deviation because of the bias induced by outliers in the dataset (Fig. 4). The MORB and WPB-like samples show systematic decrease in LOI from greenschist (median = 2.97 wt%) to lower amphibolite (median = 1.26 wt%) and upper amphibolite facies (median = 0.76 wt%; Fig. 4). Sulfur concentration decreases systematically from greenschist (0.13 wt%) to lower amphibolite (0.10 wt%) and upper amphibolite facies (0.09 wt%), whereas C stays constant (Table 3). Similarly, As, Sn, Sb, Te, and Au concentrations decrease from greenschist (10.5 ppm, 2.05 ppm, 0.14 ppm, 0.021 ppm, and 0.84 ppb, respectively) to lower amphibolite (9.0 ppm, 1.01 ppm, 0.11 ppm, 0.020 ppm, and 0.69 ppb, respectively) and upper amphibolite facies (0.98 ppm, 0.62 ppm, 0.10 ppm, 0.010 ppm, and 0.44 ppb, respectively; Fig. 1; Table 2). Other trace elements do not show systematic variation in concentration with metamorphic grade.

Metakomatiite

Metakomatiite samples show decreasing LOI content from greenschist (12.2 wt%) to lower amphibolite (8.46 wt%) and upper amphibolite facies (3.02 wt%; Fig. 5). Carbon content in upper amphibolite-facies samples (median = 0.15 wt%) is considerably lower than in greenschist and amphibolite-facies samples (median = 1.32 and 1.72 wt%, respectively; Fig. 5; Table 3). Sulfur content does not show systematic changes with metamorphism. Cobalt and Ni concentrations decrease slightly from greenschist (93.7 ppm and 656 ppm, respectively) to lower amphibolite (93.5 ppm and 627 ppm, respectively) and upper amphibolite facies (89.6 ppm and 482 ppm, respectively; Fig. 5; Table 3). Gold does not show systematic changes in concentration with metamorphism although upper amphibolite-facies samples have lower

Table 3 Whole rock composition of the metavolcanic rocks, metasedimentary rocks, and metakomatiites at different metamorphic grades

		LOI wt%	S wt%	C wt%	Co ppm	Cu ppm	As ppm	Se ppm	Mo ppm	Sn ppm	Sb ppm	Te ppm	Au ppb	U ppm
Metavolcanic and metavolcanoclastic rocks (MORB and WPB composition)														
Greenschist	Mean	3.49	0.17	0.38	51.81	96.90	15.9	0.69	1.53	5.88	0.26	0.024	1.85	0.82
	σ	1.81	0.14	0.45	7.17	57.01	17.7	0.25	0.87	10.26	0.33	0.010	2.97	0.74
	Median	**2.97**	**0.13**	**0.28**	**49.95**	**92.24**	**10.5**	**0.72**	**1.04**	**2.05**	**0.14**	**0.021**	**0.84**	**0.44**
Lower amphibolite	Mean	1.43	0.15	0.37	46.55	57.48	25.4	0.55	0.62	1.11	0.20	0.024	1.76	0.63
	σ	1.19	0.18	0.32	13.19	47.70	30.3	0.35	0.64	0.88	0.21	0.017	2.27	0.60
	Median	**1.26**	**0.10**	**0.35**	**44.71**	**55.58**	**9.0**	**0.41**	**0.56**	**1.01**	**0.11**	**0.020**	**0.69**	**0.42**
Upper amphibolite	Mean	1.09	0.11	0.27	47.89	83.85	1.44	0.61	0.84	0.71	0.15	0.014	0.87	0.93
	σ	0.83	0.11	0.26	9.39	65.04	1.18	0.24	0.55	0.63	0.14	0.011	0.98	0.82
	Median	**0.76**	**0.09**	**0.14**	**46.02**	**92.08**	**0.98**	**0.66**	**0.74**	**0.62**	**0.10**	**0.010**	**0.44**	**0.51**
Komatiites														
Greenschist	Mean	11.78	0.096	2.02	95.8	10.7	1.20	0.18	0.06	0.16	0.19	1.85	0.60	0.04
	σ	5.25	0.094	1.94	13.4	12.0	0.96	0.09	0.05	0.10	0.06	4.87	0.36	0.02
	Median	**12.20**	**0.085**	**1.32**	**93.7**	**4.2**	**0.85**	**0.15**	**0.05**	**0.12**	**0.19**	**0.007**	**0.43**	**0.03**
Lower amphibolite	Mean	9.21	0.029	1.86	92.8	31.0	1.85	0.18	1.44	0.11	0.11	0.008	1.07	0.03
	σ	2.13	0.045	0.44	5.3	38.7	1.56	0.08	2.43	0.00	0.00	0.002	1.03	0.00
	Median	**8.48**	**0.003**	**1.72**	**93.5**	**9.6**	**1.82**	**0.17**	**0.07**	**0.11**	**0.11**	**0.007**	**0.65**	**0.03**
Upper amphibolite	Mean	2.50	0.089	0.20	77.5	46.8	0.97	0.18	0.12	0.14	0.13	0.006	0.48	0.45
	σ	0.94	0.130	0.13	24.8	39.2	0.65	0.18	0.09	0.05	0.02	0.000	0.50	0.91
	Median	**3.02**	**0.022**	**0.15**	**89.6**	**41.8**	**0.91**	**0.12**	**0.10**	**0.10**	**0.12**	**0.006**	**0.28**	**0.03**
Metasedimentary rocks (S + C > 1 wt%)														
Greenschist	Mean	7.89	5.60	2.86	101	487	127	5.5	13.4	1.91	8.16	0.30	2.88	7.25
	σ	4.06	6.13	1.89	162	512	219	7.1	16.2	1.28	18.81	0.39	7.17	7.71
	Median	**6.61**	**3.02**	**2.36**	**50**	**373**	**56**	**2.3**	**11.3**	**1.45**	**1.51**	**0.08**	**0.57**	**4.84**
Lower amphibolite	Mean	7.37	4.77	4.41	52	238	51.8	13.4	34.6	2.28	0.91	0.14	0.44	14.02
	σ	3.54	3.85	4.30	38	213	75.5	17.4	35.2	1.50	0.41	0.12	0.44	14.16
	Median	**5.01**	**4.79**	**2.22**	**40**	**200**	**7.8**	**6.9**	**16.8**	**2.10**	**1.09**	**0.09**	**0.29**	**5.65**
Upper amphibolite	Mean	4.67	1.58	1.49	62	123	4.1	4.0	9.07	0.54	0.12	0.05	0.91	3.38
	σ	2.65	3.11	1.09	32	65	4.0	8.0	20.8	0.15	0.04	0.09	0.84	5.83
	Median	**3.73**	**0.21**	**1.07**	**55**	**109**	**2.3**	**0.8**	**0.61**	**0.54**	**0.10**	**0.01**	**0.63**	**1.20**

Au concentrations (median = 0.28 ppb) than greenschist and lower amphibolite-facies samples (0.43 and 0.65 ppb, respectively).

Sulfur and C-rich metasedimentary rocks

The various metasedimentary rocks of the Kittilä Group and the Savukoski Group are referred as to S and C-rich metasedimentary rocks (S + C > 1 wt%) and have decreasing LOI content from greenschist (6.61 wt%) to lower amphibolite (5.01 wt%) and upper amphibolite facies (3.73 wt%; Fig. 6; Table 3). Carbon content shows systematic decrease from greenschist (2.36 wt%) to lower amphibolite (2.22 wt%) and upper amphibolite facies (1.07 wt%) whereas S shows considerably lower concentration in upper amphibolite-facies samples (median = 0.21 wt%) than in greenschist (3.02 wt%) and lower amphibolite-facies samples (4.79 wt%; Table 3). Copper, As, and Sb show systematic decrease in concentration from greenschist (373 ppm, 56 ppm, and 1.51 ppm, respectively) to lower amphibolite (200 ppm, 7.8 ppm, and 1.09, respectively) and upper amphibolite facies (109 ppm, 2.3 ppm, and 0.10 ppm, respectively; Fig. 6; Table 3). Selenium, Mo, Sn, Te, and U have considerably lower concentrations in upper amphibolite-facies samples (0.77 ppm, 0.61 ppm, 0.54 ppm, 0.01 ppm, and 1.20 ppm, respectively) than in greenschist (2.33 ppm, 11.3 ppm, 1.45 ppm, 0.08 ppm, and 4.84 ppm, respectively) and lower amphibolite-facies

Journal : Large 126 | Article No : 1133 | Pages : 28 | MS Code : 1133 | Dispatch : 10-9-2022

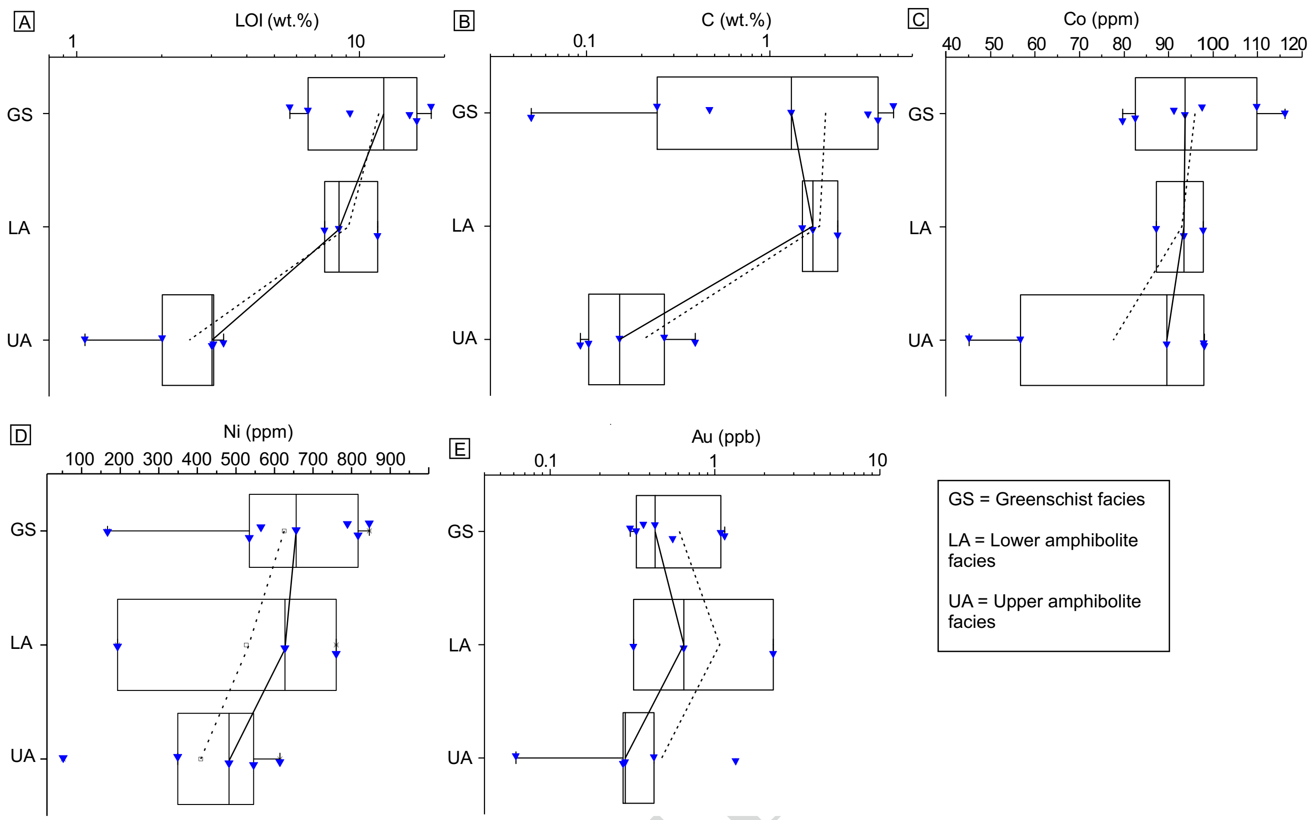

Fig. 5 **A** LOI, **B** C, **C** Co, **D** Ni and **E** Au content in metakomatiites from the Savukoksi Group according to their metamorphic facies. Only elements showing systematic variation in composition with metamorphic grade are shown. Box range and lines as in Fig. 4

samples (6.94 ppm, 16.8 ppm, 2.10 ppm, 0.09 ppm, and 5.65 ppm, respectively; Table 3). Gold and Co do not show systematic decrease relative to metamorphic grade (Fig. 6).

Protolith composition

There are three critical parameters for determining the potential of lithological units as metal source: (1) the primary content of the elements of interest at the onset of metamorphism (defined as the metamorphic protolith composition), (2) the degree of depletion, and (3) the volume of the unit. The metamorphic protolith composition and the volume of the unit buffer the quantity of element availability for hydrothermal mobilization and can be referred to as the metal fertility. The degree of depletion is dependent on the efficiency of hydrothermal fluids in mobilizing the elements out of the source rock. This efficiency is related to the degree of disequilibrium between the fluids and the rocks, which is dependent on the physicochemical characteristics of both the hydrothermal fluids and the rocks. The degree of depletion is inferred through mass variation calculations between protolith and altered rocks (Pitcairn et al. 2006a; Jowitt et al. 2012; Patten et al. 2016). A lithological unit has a high potential as a source if it has both a high metal fertility and is highly depleted.

Metavolcanic rocks with MORB and WPB signature

To determine the mass variations related to metamorphic devolatilization, the different protolith primary composition before the onset of metamorphism must be characterized. Metamorphic protolith composition, however, is notoriously difficult to determine due to the numerous processes that affected trace element concentration before onset of metamorphism. Trace element contents in MORB and WPB-like samples are controlled by differences in mantle source, magmatic processes, and seafloor alteration preceding metamorphism (Tatsumi et al. 1999; Jenner and O'Neill 2012; Webber et al. 2013; Patten et al. 2016). Comparison with modern-day fresh glass MORB and WPB can provide insights into protolith composition, especially for elements which are poorly affected by low-temperature seafloor alteration such as Au (Nesbitt et al. 1987; Pitcairn et al. 2015; Patten et al. 2016). Their use as proxies for metamorphic protolith composition, however, is limited as the differences in mantle source and magmatic differentiation between

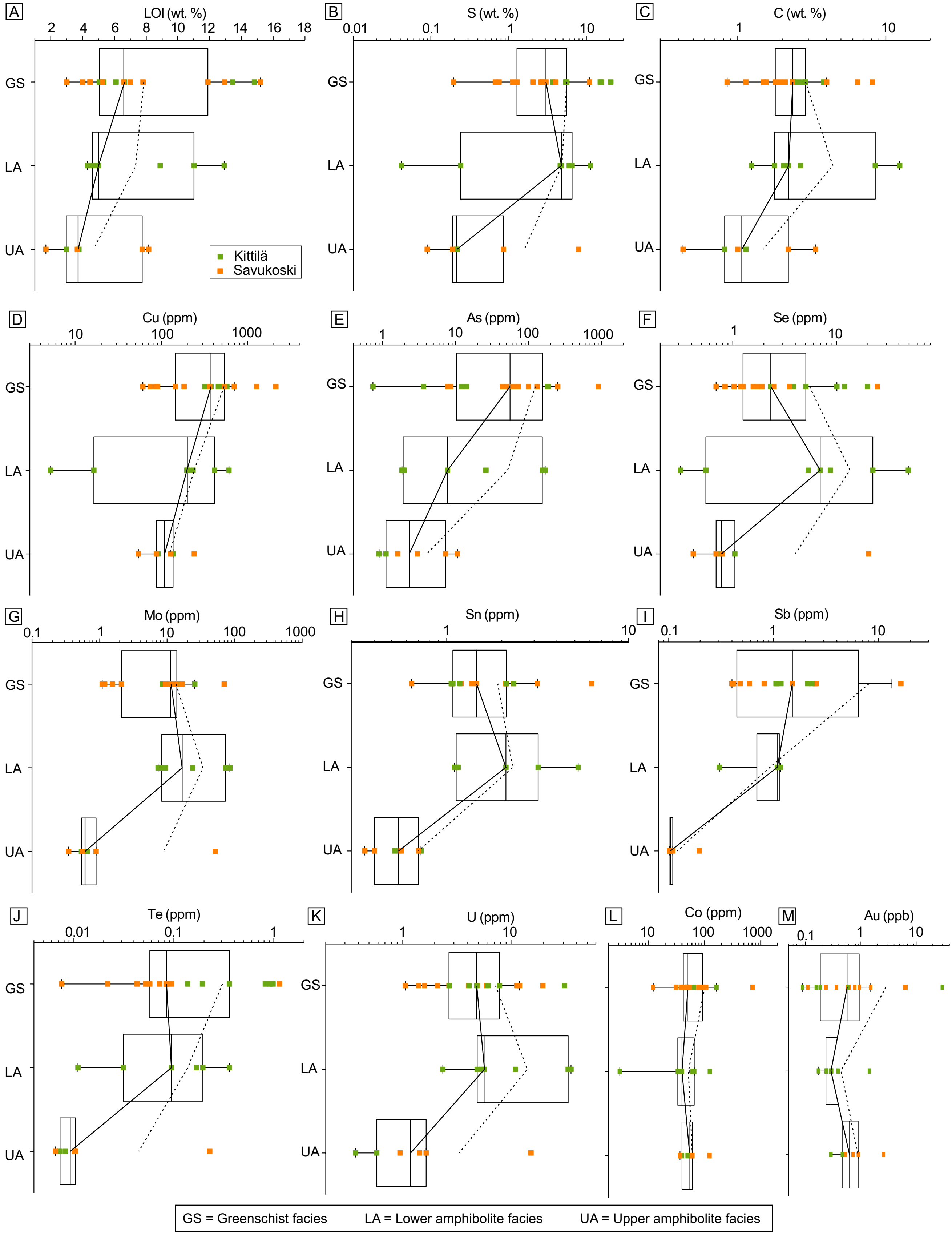

Fig. 6 **A** LOI, **B** S, **C** C, **D** Cu, **E** As, **F** Se, **G** Mo, **H** Sn, **I** Sb, **J** Te, **K** U, **L** Co, and **M** Au content in metasedimentary rocks (S + C > 1 wt%) from the Kittilä and Savukoski groups according to their metamorphic facies. Box range and lines as in Fig. 4

Journal : Large 126	Article No : 1133	Pages : 28	MS Code : 1133	Dispatch : 10-9-2022

Precambrian and modern-day MORB and WPB, and related effect on trace element concentration, are not well constrained (Patten et al. 2020). For instance, MORB and WPB from the CLGB show evidence of contamination from the Archean basement via the assimilation-fractionation-crystallization mechanism (Hanski and Huhma 2005; Patten et al. 2020), but the impact on trace element concentration is difficult to estimate. Thus, MORB- and WPB-like samples metamorphosed at greenschist facies are considered better proxies for the metamorphic protolith composition. They have sustained the same magmatic-hydrothermal history as their higher metamorphic grade counterparts, enabling direct comparison, and trace element mobility during sub-greenschist-facies metamorphism can be considered limited (Pitcairn et al. 2006a, 2015). Patten et al. (2020) highlighted that magmatic differentiation trends for Au in MORB and WPB are preserved in greenschist-facies samples from the CLGB, enabling improved characterization of the protolith composition. The Zr/Y ratio, which is not affected by seafloor alteration and sub-greenschist facies metamorphism, is used to differentiate between MORB and WPB magmatic trends. This approach, however, does not work for other elements, which also show systematic decrease with increasing metamorphic grade, such as S, As, Sn, and Sb, as no magmatic differentiation trends are preserved in greenschist-facies samples. These elements have relatively high mobility during low-temperature seafloor alteration (Alt 1995; Jochum and Verma 1996; Patten et al. 2016) preventing preservation of magmatic trends. Hence, the median values of the greenschist facies samples are used as proxies for the metamorphic protolith composition (S = 0.13 wt%, As = 10.5 ppm, Sn = 2.05 ppm, and Sb = 0.14 ppm; Table 3).

Sulfur and C-rich metasedimentary rocks

Trace element content in S and C-rich metasedimentary rocks is highly variable, depending on sediment source and diagenetic processes (Crocket 1993; Ketris and Yudovich 2009; Large et al. 2011; Pitcairn 2011). Sulfide content in metasedimentary rocks of the CLGB has a strong control on Cu, Se, Mo, Sb, Te, and U but limited control on Co, As, Sn, and Au (Figs. 6 and 7). Trace element content in the metamorphic protolith is thus strongly controlled by the primary sulfide content for some elements, and their distribution in variably metamorphosed samples might reflect differences in protolith sulfide content rather than mobilization due to metamorphism. To circumvent this problem, the Co/Mo ratio can be used (Fig. 8). Cobalt and Mo are both hosted by sulfides in metasedimentary rocks (Pitcairn et al. 2006a; Large et al. 2011, 2014; Hu et al. 2016), but during metamorphism, Co is redistributed between sulfide phases, from pyrite to cobaltite and pyrrhotite (Pitcairn et al. 2006a; Large et al. 2014), and

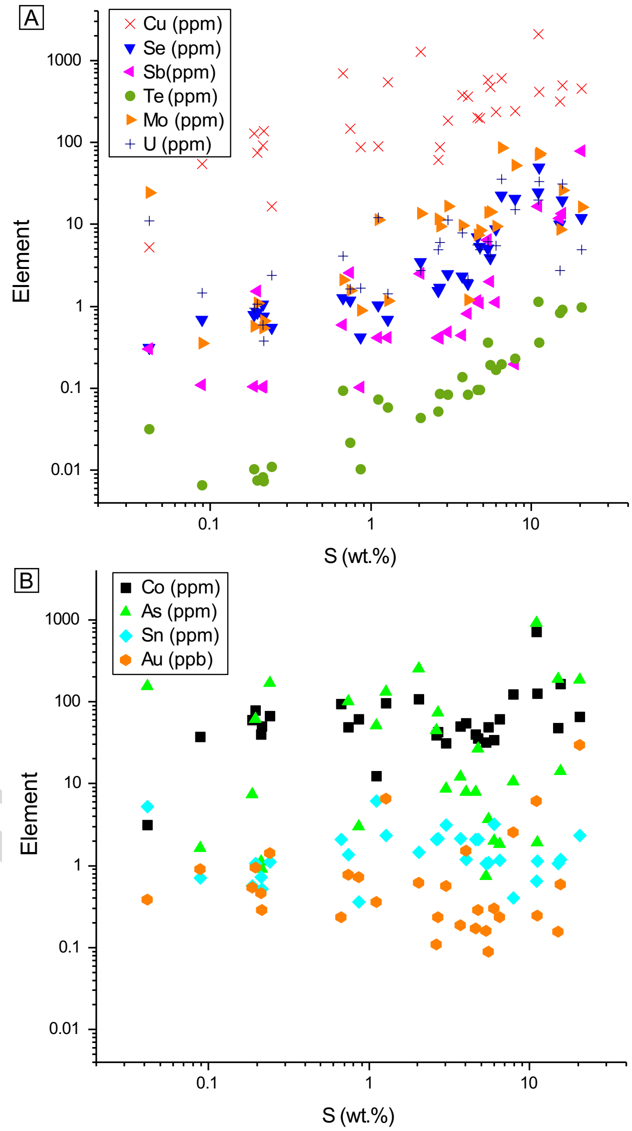

Fig. 7 Trace element content versus S in the metasedimentary rocks from the Kittilä and Savukoski groups. **A** Cu, Mo, Se, Sb, Te, and U show strong correlation with sulfide content whereas **B** Co, As, Sn, and Au do not

can be considered as an immobile element if the metamorphic fluids have relatively low salinity (Fig. 6; Qiu et al. 2021), whereas Mo is efficiently mobilized, showing a similar behavior to S (Large et al. 2011, 2014; Fig. 6). Increasing devolatilization thus leads to increase in the Co/Mo ratio independently of the primary sulfide content (Fig. 8). Correlation of Se, Cu, Sb, Te, and U with the Co/Mo ratio implies that trace element variation is related to metamorphic grade rather than to primary sulfide content. Although some trace element mobility in metasedimentary rocks can occur early before greenschist-facies

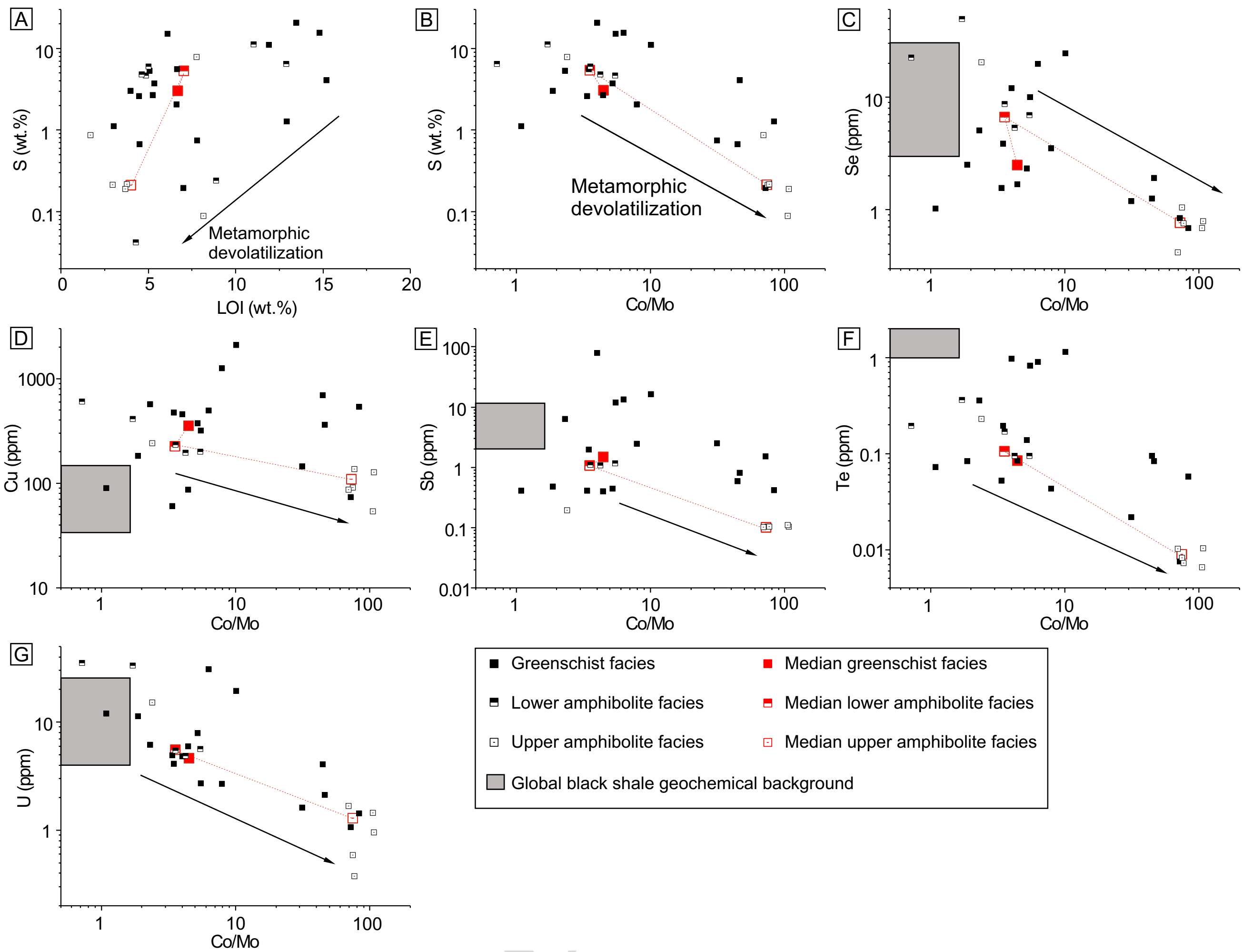

Fig. 8 **A** S vs LOI and **B** S, **C** Se, **D** Cu, **E** Sb, **F** Te, and **G** U vs Co/Mo in metasedimentary rock samples from the Kittilä and Savukoski groups. Increase in Co/Mo ratio indicates metamorphic devolatilization. Geochemical background of global black shales defined by Ketris and Yudovich (2009)

metamorphism (Large et al. 2011; Pitcairn et al. 2006a), the median of greenschist-facies samples is used as proxy for protolith composition (Table 3). Greenschist-facies median values of Co, Cu, As, Se, Mo, Sn, Sb, Te, and U (50 ppm, 373 ppm, 56 ppm, 2.3 ppm, 11.3 ppm, 1.45 ppm, 1.51 ppm, 0.08 ppm, and 4.84 ppm, respectively; Table 3) are comparable to the global median values in black shale as determined by Ketris and Yudovich (2009; 19 ppm, 70 ppm, 30 ppm, 8.7 ppm, 20 ppm, 3.9 ppm, 5.0 ppm, 2.0 ppm, and 8.5 ppm, respectively; Fig. 8). The Cu concentration (373 ppm), however, is considerably higher than the global black shale median (70 ppm), whereas Te (0.08 ppm) and Au (0.57 ppb) concentrations are considerably lower (2.0 ppm and 7 ppb, respectively; Ketris and Yudovich 2009). The discrepancy for Au can possibly be attributed to unfavorable conditions for Au incorporation during sedimentation and diagenesis such as low Au content in seawater at 2.0–1.6 Ga (Large et al. 2015).

Metakomatiite

The trace element content in metakomatiite protolith is controlled by complex processes such as mantle source, degree of mantle melting, melt contamination by supra-crustal rocks, possible sulfide segregation, and seafloor alteration (Barnes and Often 1990; Hanski et al. 2001b; Schandl and Gorton 2012; Heggie et al. 2013). The limited number of metakomatiite samples metamorphosed at greenschist facies ($n=7$) makes the characterization of trace element distribution in the protolith difficult. The dataset is completed by whole rock data from the Karasjok greenstone belt (Barnes and Often 1990), the northern prolongation of the CLGB in Norway, and from the Peuramaa and Jeesiörova localities along the SiSZ (Hanski et al. 2001b). These rocks, although showing some differences in major element concentration (e.g., the Karasjok komatiites are more TiO_2–rich), share

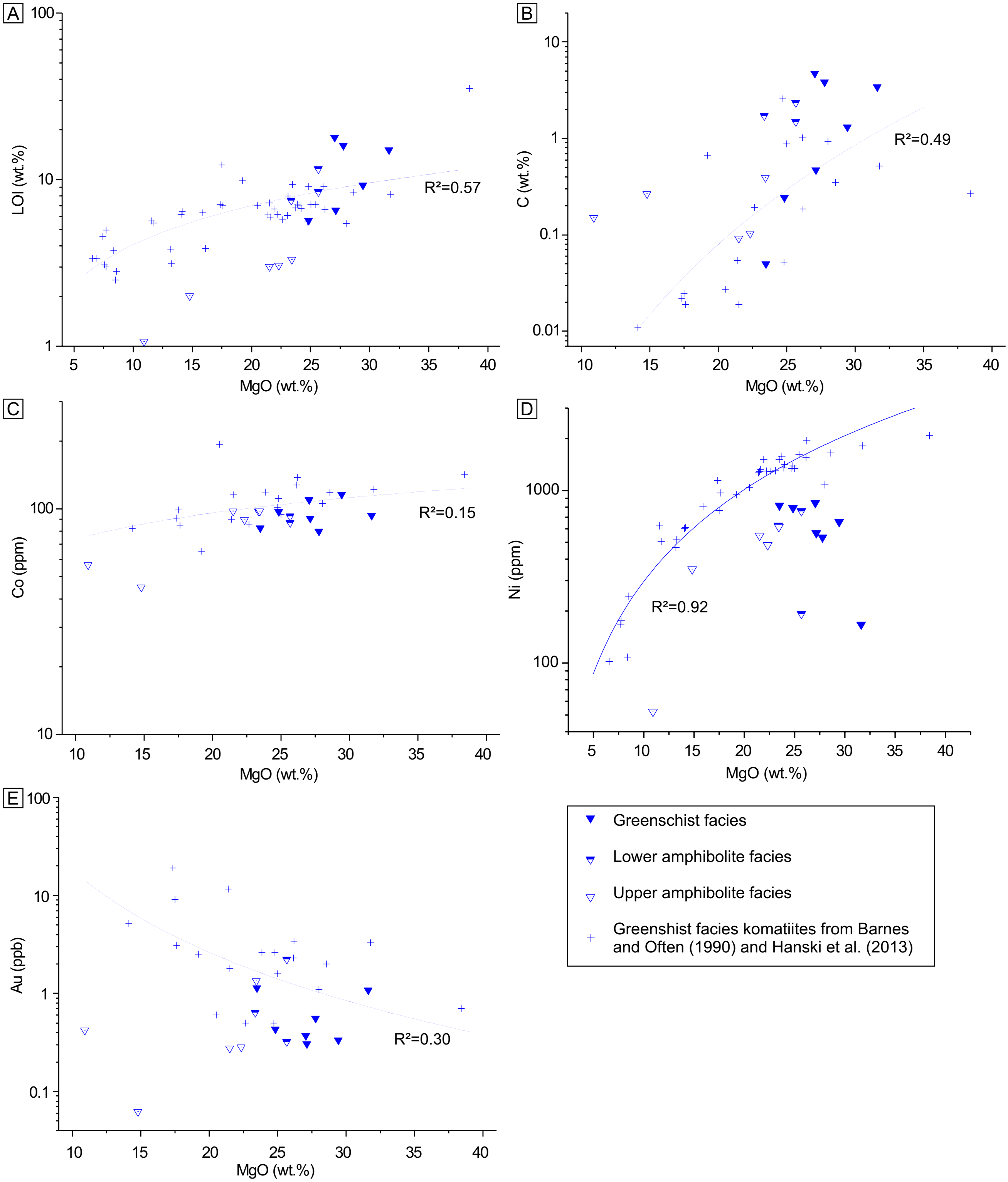

Fig. 9 LOI, C, Co, Ni, and Au content relative to MgO in the meta-komatiites from the Savukoski Group. The trend lines are the calculated protolith composition using greenschist facies samples from this study and from Barnes and Often (1990) and Hanski et al. (2013; blue crosses) except for Ni (see text). GS = greenschist, LA = lower amphibolite, UA = upper amphibolite

Journal : Large 126	Article No : 1133	Pages : 28	MS Code : 1133	Dispatch : 10-9-2022

the same genetic processes to the rocks from this study (Lehtonen et al. 1998; Hanski et al. 2001b), and they were metamorphosed only up to greenschist facies (Barnes and Often 1990). Using these data, magmatic differentiation curves were calculated for Co and Au using MgO (Fig. 9). Nickel concentrations in metakomatiite from this study are lower than those from Barnes and Often (1990), and Hanski et al. (2001b) and do not show clear magmatic differentiation trends. However, the low Ni concentration of upper amphibolite-facies samples relative to greenschist and lower amphibolite facies samples (Fig. 5) is nevertheless partly due to magmatic differentiation as they are characterized by low MgO content (Fig. 9). Nickel distribution in metakomatiite thus cannot be attributed to either magmatic or metamorphic processes, and mass variation related to metamorphism cannot be calculated. The metakomatiite samples are characterized by relatively high LOI and C (Table 1), most likely due to serpentinization and carbonation during seafloor alteration (Barnes and Often 1990; Schandl and Gorton 2012), but LOI and C show nevertheless correlation with MgO (Fig. 9). The calculated trends for the LOI, C, Co, and Au are used as proxies for the metamorphic protolith composition (Fig. 9), whereas the median values of greenschist-facies samples are used as the metamorphic protolith composition for the other elements of interest (Table 3).

Table 4 Mass variation calculations for selected elements at greenschist, lower amphibolites, and upper amphibolite-facies conditions relative to protolith composition

		LOI wt%	S wt%	C wt%	Co ppm	Cu ppm	As ppm	Se ppm	Mo ppm	Sn ppm	Sb ppm	Te ppm	Au* ppb	U ppm
Metavolcanic and metavolcanoclastic rocks (MORB and WPB composition)														
Greenschist	Mean	17.3	22.9	54.1	4.6	3.7	49.3	−2.8	47.3	187.7	81.2	5355	94.1	78.4
	σ	60.9	112.6	186.0	15.4	58.7	167.9	43.6	83.5	501.5	234.9	19,978	393.6	172.9
	Median	**0**	**0**	**0**	**0**	**0**	**0**	**0**	**0**	**0**	**0**	**0**	**−14.8**	**0**
Lower amphibolite	Mean	−51.8	13.9	55.6	−4.5	−39.3	146.0	−17.0	−40.6	−45.7	40.8	17.4	153.9	46.1
	σ	40.2	141.6	136.6	27.1	50.4	293.6	52.2	61.5	42.8	147.5	83.2	312.0	138.7
	Median	**−57.6**	**−18.5**	**46.4**	**−8.3**	**−41.3**	**−12.2**	**−38.8**	**−46.1**	**−50.4**	**−21.5**	**−2.9**	**14.0**	**−1.7**
Upper amphibolite	Mean	−65.4	−16.6	1.7	−1.0	−10.2	−85.9	−11.7	−18.4	−65.3	9.7	−31.8	−21.2	121.9
	σ	27.5	86.2	104.6	19.6	70.7	11.8	34.9	54.3	31.7	97.5	55.3	96.4	194.5
	Median	**−75.8**	**−45.6**	**−44.7**	**−2.7**	**−1.6**	**−90.9**	**−6.7**	**−33.8**	**−71.5**	**−28.5**	**−51.3**	**−58.7**	**30.7**
Komatiites														
Greenschist	Mean	29.3	185.3	243.0	−11.8	−71.8	41.0	19.7	15.1	39.0	−1.6	6.7	−43.2	17.3
	σ	56.7	277.5	374.4	11.6	31.5	111.9	60.4	102.6	86.9	29.9	20.8	43.0	49.9
	Median	**25.2**	**151.6**	**72.2**	**−15.8**	**−88.8**	**0.0**	**0.0**	**0.0**	**0.0**	**0.0**	**0.0**	**−62.6**	**0.0**
Lower amphibolite	Mean	11.0	−14.8	560.2	−11.3	−18.4	116.3	17.2	2790.7	−7.2	−43.0	10.8	−21.8	−5.9
	σ	22.7	133.4	213.8	6.7	102.0	182.5	49.9	4875.0	1.9	1.2	33.5	81.5	1.9
	Median	**0.1**	**−91.0**	**582.4**	**−11.9**	**−74.8**	**112.5**	**10.4**	**30.7**	**−8.2**	**−43.6**	**−7.0**	**−61.9**	**−6.8**
Upper amphibolite	Mean	−63.1	164.0	1661.1	−17.8	23.3	13.7	17.7	137.9	13.9	−35.2	−12.5	−77.8	1175.0
	σ	7.2	385.1	2786.5	19.0	103.2	76.3	118.0	181.3	38.5	11.9	6.6	32.5	2590.4
	Median	**−59.7**	**−34.1**	**95.2**	**−10.8**	**10.0**	**6.4**	**−19.2**	**106.9**	**−12.7**	**−37.2**	**−14.8**	**−87.0**	**−11.5**
Metasedimentary rocks (S + C > 1 wt%)														
Greenschist	Mean	19.6	19.4	85.4	21.2	30.3	30.4	127.3	137.2	18.3	31.5	440.2	257.8	404.6
	σ	26.2	61.5	202.6	80.0	92.8	137.2	394.1	303.8	142.9	88.3	1244.6	461.6	1257.9
	Median	**5.5**	**0.0**	**0.0**	**0.0**	**0.0**	**0.0**	**0.0**	**0.0**	**0.0**	**0.0**	**0.0**	**0.0**	**0.0**
Lower amphibolite	Mean	3.1	11.5	57.9	87.0	198.0	−36.2	−6.9	473.9	204.9	57.1	−39.5	61.6	−23.5
	σ	1.9	53.6	127.4	182.6	246.7	56.9	135.7	749.6	310.6	103.4	27.1	140.8	77.4
	Median	**3.6**	**−24.2**	**58.4**	**−6.0**	**93.9**	**−46.5**	**−86.0**	**198.2**	**47.7**	**44.6**	**−27.6**	**12.1**	**−49.1**
Upper amphibolite	Mean	72.5	−29.3	−47.8	−36.8	112.4	−67.2	−92.6	73.0	−20.0	−62.5	−92.1	−46.5	59.9
	σ	37.9	40.1	102.8	46.3	381.8	17.4	7.1	345.7	183.0	10.3	2.5	106.3	146.5
	Median	**75.6**	**−43.6**	**−92.9**	**−54.8**	**−31.3**	**−70.9**	**−95.8**	**−66.7**	**−94.6**	**−62.7**	**−93.1**	**−89.1**	**10.4**

*Au mass variation calculations in MORB and WPB are from Patten et al. (2020)

Journal : Large 126 | Article No : 1133 | Pages : 28 | MS Code : 1133 | Dispatch : 10-9-2022

Table 5 Mann–Whitney statistical test. Mass variations are significant when the null hypothesis is rejected

		LOI wt%	S wt%	C wt%	Co ppm	Cu ppm	As ppm	Se ppm	Mo ppm	Sn ppm	Sb ppm	Te ppm	Au ppb	U ppm
Metavolcanic and metavolcanoclastic rocks (MORB and WPB composition)														
Greenschist	**Median**	**0.00**	**0.00**	**0.00**	**0.00**	**0.00**	**0.00**	**0.00**	**0.00**	**0.00**	**0.00**	**0.00**	**−14.8**	**0.00**
	p value	1	1	1	1	1	1	1	1	1	1	1	0.53	1
	Null hypothesis	Not rejected	Not rejected	Not rejected	Not rejected	Not rejected	Not rejected	Not rejected	Not rejected	Not rejected	Not rejected	Not rejected	Not rejected	Not rejected
Lower amphibolite	**Median**	**−57.6**	**−18.5**	**46.4**	**−8.3**	**−41.3**	**−12.2**	**−38.8**	**−46.1**	**−50.4**	**−21.5**	**−2.9**	**14.0**	**−1.7**
	p value	**6.50E−05**	0.35	0.62	0.22	**0.02**	0.87	0.16	0.03	**7.67E−04**	0.55	0.20	0.18	0.73
	Null hypothesis	**Rejected**	Not rejected	Not rejected	Not rejected	**Rejected**	Not rejected	Not rejected	Not rejected	**Rejected**	Not rejected	Not rejected	Not rejected	Not rejected
Upper amphibolite	**Median**	**−75.8**	**−45.6**	**−44.7**	**−2.7**	**−1.6**	**−90.9**	**−6.7**	**−33.8**	**−71.5**	**−28.5**	**−51.3**	**−58.7**	**30.7**
	p value	**1.20E−05**	0.20	0.79	0.41	0.62	**5.10E−04**	0.66	0.28	**3.60E−05**	0.21	**2.30E−04**	**0.041**	0.34
	Null hypothesis	**Rejected**	Not rejected	Not rejected	Not rejected	Not rejected	**Rejected**	Not rejected	Not rejected	**Rejected**	Not rejected	**Rejected**	**Rejected**	Not rejected
Komatiites														
Greenschist	**Median**	**25.2**	**151.61**	**72.16**	**−15.8**	**−88.8**	**0.0**	**0.0**	**0.0**	**0.0**	**0.0**	**0.0**	**−62.6**	**0.0**
	p value	0.44	0.97	0.28	0.085	**0.018**	1	1	1	1	1	1	0.064	1
	Null hypothesis	Not rejected	Not rejected	Not rejected	Not rejected	**Rejected**	Not rejected	Not rejected	Not rejected	Not rejected	Not rejected	Not rejected	Not rejected	Not rejected
Lower amphibolite	**Median**	**0.1**	**−91.0**	**582**	**−11.9**	**−75**	**113**	**10.4**	**30.7**	**−8.2**	**−43.6**	**−7.0**	**−61.9**	**−6.8**
	p value	0.43	0.077	0.05	0.19	0.41	0.34	0.63	0.90	0.24	**0.028**	0.70	0.37	0.52
	Null hypothesis	Not rejected	Not rejected	Not rejected	Not rejected	Not rejected	Not rejected	Not rejected	Not rejected	Not rejected	**Rejected**	Not rejected	Not rejected	Not rejected
Upper amphibolite	**Median**	**−59.7**	**−34.1**	**95.2**	**−10.8**	**10**	**6.4**	**−19.2**	**106.9**	**−12.7**	**−37.2**	**−14.8**	**−87.0**	**−11.5**
	p value	**2.63E−04**	1.0	0.11	0.072	0.470	1.00	0.33	0.24	0.32	0.06	0.036	**3.40E−03**	0.52
	Null hypothesis	**Rejected**	Not rejected	Not rejected	Not rejected	Not rejected	Not rejected	Not rejected	Not rejected	Not rejected	Not rejected	Not rejected	**Rejected**	Not rejected
Metasedimentary rocks (S + C > 1 wt%)														
Greenschist	**Median**	**0.0**	**0.0**	**0.0**	**0.0**	**0.0**	**0.0**	**0.0**	**0.0**	**0.0**	**0.0**	**0.0**	**0.0**	**0.0**
	p value	1	1	1	1	1	1	1	1	1	1	1	1	1
	Null hypothesis	Not rejected	Not rejected	Not rejected	Not rejected	Not rejected	Not rejected	Not rejected	Not rejected	Not rejected	Not rejected	Not rejected	Not rejected	Not rejected
Lower amphibolite	**Median**	**−24.2**	**58.4**	**−6.0**	**−19.6**	**−46.5**	**−86.0**	**198.2**	**47.7**	**44.6**	**−27.6**	**12.1**	**−49.1**	**16.6**
	p value	0.6	0.9	0.8	0.4	0.3	0.2	0.5	0.3	0.6	0.4	1.0	0.7	0.2
	Null hypothesis	Not rejected	Not rejected	Not rejected	Not rejected	Not rejected	Not rejected	Not rejected	Not rejected	Not rejected	Not rejected	Not rejected	Not rejected	Not rejected
Upper amphibolite	**Median**	**−43.6**	**−92.9**	**−54.8**	**11.0**	**−70.9**	**−95.8**	**−66.7**	**−94.6**	**−62.7**	**−93.1**	**−89.1**	**10.4**	**−75.2**
	p value	**0.074**	**0.022**	**0.046**	1	**0.039**	**0.0057**	**0.039**	**0.016**	**6.80E−04**	**4.10E−04**	**0.013**	0.55	**0.032**
	Null hypothesis	**Rejected**	**Rejected**	**Rejected**	Not rejected	**Rejected**	**Rejected**	**Rejected**	**Rejected**	**Rejected**	**Rejected**	**Rejected**	Not rejected	**Rejected**

Element depletion during metamorphism

Element depletion of a source is determined using mass variation calculation. Mass variation in trace elements due to prograde metamorphism is defined as the difference between the metamorphic protolith composition and metamorphosed sample:

$$\Delta E = E_p - E_s$$

where ΔE is the element's mass variation, E_p the protolith composition, and E_s the element concentration in the sample of interest. The metamorphic protolith composition is either the median of the greenschist-facies sample or the value determined from differentiation trends when possible (i.e., metakomatiite; Fig. 9). Mass variations for trace elements in greenschist, lower amphibolites, and upper amphibolite facies are compiled in Table 4 for each lithological group. To determine the significance of the calculated mass variations, a Mann–Whitney test for non-normal distribution is used. The null hypothesis specifies no statistical differences relative to the protolith at 0.05 confidence level (Table 5).

Metavolcanic rocks with MORB and WPB signature

Significant mass variation between the lower amphibolite facies and the protolith occurs for the LOI (−57.6%), Cu (−60.3%), and Sn (−50.4%). At the upper amphibolite facies, significant mass variation occurs for the LOI (−75.8%), As (−90.9%), Sn (−71.5%), and Au (−58.7%; Table 5). Systematic and increasing depletion of LOI relative to the protolith, from greenschist to upper amphibolite facies, highlights the devolatilization during prograde metamorphism. Sulfur and C do not show significant mass variations although S mass variation in upper amphibolite-facies samples (median = −45.6%) is significant with a 80% degree of confidence (p value = 0.2; Table 5). A larger dataset would allow to better understand S mobility during metamorphism of MORB and WPB. Arsenic and Au mass variations are significant in the upper amphibolite facies (median = −90.9% and −58.7%, respectively), whereas Sn mass variations are significant in both the lower amphibolite and upper amphibolite facies (median = −50.4% and −71.5%, respectively), implying efficient mobilization of As, Sn, and Au during upper amphibolite-facies metamorphism. Efficient mobilization of As from the metavolcanic rocks is inconsistent with the findings of Pitcairn et al. (2015), which show no As mobilization from metavolcanic rocks of the thick Otago Schist metasedimentary sequence but rather As enrichment. A possible explanation for this discrepancy is that the metavolcanic rocks of the Otago schists interacted with the As-rich metamorphic fluids sourced from the surrounding and voluminous metasedimentary rocks (~95% vol. of the sequence; Pitcairn et al. 2015). In the CLGB, mass variation of Cu is significant in the lower amphibolite facies but not in the upper amphibolite facies, implying that Cu distribution is possibly not solely controlled by prograde metamorphic devolatilization but by cryptic magmatic processes and, therefore, is not considered further here.

Metasedimentary rocks

Significant mass variation in S- and C-rich metasedimentary rocks relative to the metamorphic protolith composition occurs for the LOI (−43.6%), S (−92.9%), C (−54.8%), Cu (−70.9%), As (−95.8%), Se (−66.7%), Mo (−94.6%), Sn (−62.7%), Sb (−93.1%), Te (−89.1%), and U (−75.2%) at the upper amphibolite facies (Table 5). Gold does not show any significant mass variation. The lack of Au mass variation is partly explained by the low Au content of the metamorphic protolith.

Metakomatiite

Relative to the protolith composition, significant mass variation in metakomatiite occurs for Cu in the greenschist facies (−88.8%), for Sb at the lower amphibolite facies (−43.6%), and for the LOI and Au at the upper amphibolite facies (−59.7% and −87%, respectively). Cobalt does not show significant mass variation (Fig. 9; Table 5). The Cu mass variation in the greenschist facies is related to the lower Cu content of the metakomatiites of this study (median = 4.2 ppm) relative to those of Barnes and Often (1990; median = 74.5 ppm) rather than to metamorphism. The reasons for such low values are not understood. The mass variation of LOI and Au, although statistically significant, should be interpreted carefully as the metakomatiite sample population is relatively small (n = 15).

Control of the source on metal endowment in orogenic Au deposits

Mass balance calculation

The 3D shape of the Kittilä Group rock package has been modeled using aeromagnetic and gravity maps as well as seismic profiles, revealing a hull shape with a maximum thickness of 9.5 km in the center and thinning out towards the margins (Fig. 10; Niiranen et al. 2015). The substantial thickening occurred via thrust stacking during D1–D2 (e.g., along the KiSZ; Sayab et al. 2019). From the total of 9500 km^3 calculated for the Kittilä Group, ~1500 km^3 of rocks are inferred to be metamorphosed at the upper amphibolite facies (> 500–550 °C), representing a possible major

Journal : Large 126 | Article No : 1133 | Pages : 28 | MS Code : 1133 | Dispatch : 10-9-2022

source volume for the orogenic Au deposits hosted in the CLGB (Niiranen et al. 2015). The Kittilä Group not only is dominated by metavolcanic rocks but also hosts minor metasedimentary rocks that should be included in mass balance calculations. Assuming a similar relative proportion of metavolcanic rocks to metasedimentary rocks in the Kittilä Group at depth to that at the surface, a proportion of 99.6% to 0.4%, respectively, is determined from GTK DigiKP 1:200,000 digital geological map (Fig. 1). It is estimated that ~1494 km^3 of metavolcanic rocks and ~6 km^3 of metasedimentary rocks were metamorphosed at upper amphibolite facies. The volume of the Savukoski Group, however, is not constrained but is likely significant (Niiranen, personal communication, 2019). During the tectonic evolution, the Kittilä Group was thrust from the west onto the Savukoski Group, while to the south, the Savukoski Group was thrust onto the Kittilä Group along the SiSZ. It can be inferred, thus, that the Kittilä Group hull structure is surrounded by the Savukoski Group at depth and to the south of the SiSZ (Fig. 10) as implied from the geological map (Fig. 1). Unlike the Kittilä Group, the Savukoski rock package most likely did not sustain extensive thickening at depth due to thrust stacking making it considerably less voluminous in the source zone. We use a conservative volume of half that of the Kittilä rock package (~750 km^3). The relative proportion of metavolcanic rocks to metasedimentary rocks and metakomatiites in the Savukoski Group from the GTK DigiKP 1:200,000 digital geological map is 29.7%, 29.4%, and 40.9%, respectively. Assuming a similar ratio at depth, a volume of ~223 km^3 of metavolcanic rocks, ~220 km^3 of metasedimentary rocks, and ~307 km^3 of metakomatiites is estimated to have been metamorphosed at the upper amphibolite facies in the Savukoski Group.

Mass balance calculations were carried out for the Kittilä Group and Savukoski Group rocks using the metamorphic protolith compositions (Table 3), the calculated element mass variations (Table 4), the estimated rock volumes in the source areas, and the densities of 3003 kg/m^3 for metavolcanic rocks, 2962 kg/m^3 for metasedimentary rocks, and 2971 kg/m^3 for metakomatiite (ESM 1). The calculated mass balances are semi-quantitative as uncertainties cannot be propagated (the highest uncertainty being related to the volume of the source zones and the lithological unit proportions). They nevertheless provide insight into the order of magnitude of the element flux from the different source volumes with staggering quantities of S, C, Cu, and As (> 100 Mt), Se, Mo, Sn, and U (> 1 Mt), and Sb, Te, and Au (> 1000 t; Table 6) being mobilized. The total Au mobilized from both the Kittilä and Savukoski groups (~2500 t) is one order of magnitude higher than the reported Au resources in the CLGB orogenic Au deposit (~440 t; Mineral Deposit Database of Finland 2022). The calculated quantity of mobilized Au is lower than the 4425–7080 t Au estimated by Niiranen et al. (2015) but of the same order of magnitude, the difference being caused by the overestimated protolith Au composition (2 ppb) used by Niiranen et al. (2015). Bulk Cu endowment in the CLGB orogenic Au deposits is not well constrained, but a minimum estimate of 0.13 Mt Cu (compilation from Saattopora, Levijärvi, Tepsa, Riikoski and Sirkka deposits) implies that the total Cu mobilized from both the Kittilä Group and the Savukoski Group (~180 Mt Cu) is significantly higher than the bulk Cu endowment in the deposits. The endowments of other metals in the CLGB are even less well constrained, but it can be assumed that, similarly to Au and Cu, the metal quantities mobilized from the sources are significantly higher than the ones trapped in the deposits.

Different sources for typical and atypical orogenic Au deposits?

The different lithological proportions of metavolcanic rocks, metasedimentary rocks, and metakomatiite between the Kittilä and Savukoski groups have important control on the element quantity mobilized during metamorphic devolatilization. The metavolcanic rocks released significant Au, As, Sn, Te, and possibly S, whereas the metasedimentary rocks released significant S, C, Cu, As, Se, Mo, Sn, Sb, Te, and U and the metakomatiites released C and possibly Au. Nickel and Co do not show systematic mobilization and a clear source for Ni and Co cannot be determined. The presence of evaporites in metamorphic belts appears as important for Co mobilization either by acting as a Co source (Qiu et al. 2021) and/or by providing Cl for forming Co–Cl complexes (Brugger et al. 2016; Qiu et al. 2021). Although some metaevaporites remnants are locally present within the CLGB, they appear to be limited and restricted to the southern part of the belt (Frietsch et al. 1997), and possibly had little impact on regional scale metal mobilization. They could have, nevertheless, locally and transiently favored Co mobilization, possibly promoting some atypical mineralization (Frietsch et al. 1997). Noteworthy, the atypical orogenic Au deposits of the CLGB are rather Cu-rich than Co-rich in comparison with the Kuusamo Belt, for instance, which hosts several Au and Au–Co orogenic deposits showing evidence of mineralizing fluids with an evaporitic component (Vasilopoulos et al. 2021).

In the Kittilä Group, which is dominated by metavolcanic rocks (~99.6 vol%), the metamorphic fluids generated by devolatilization would have been preferentially enriched in Au, As, Sn, Te, and possibly S. The metasedimentary rocks, although minor (~0.4 vol%), would still have provided large quantities of S and As to the metamorphic fluids (~490 Mt S and ~0.9 Mt As; Table 6). In the Savukoksi Group, however, metasedimentary rocks represent a large volume fraction

Journal : Large 126 | Article No : 1133 | Pages : 28 | MS Code : 1133 | Dispatch : 10-9-2022

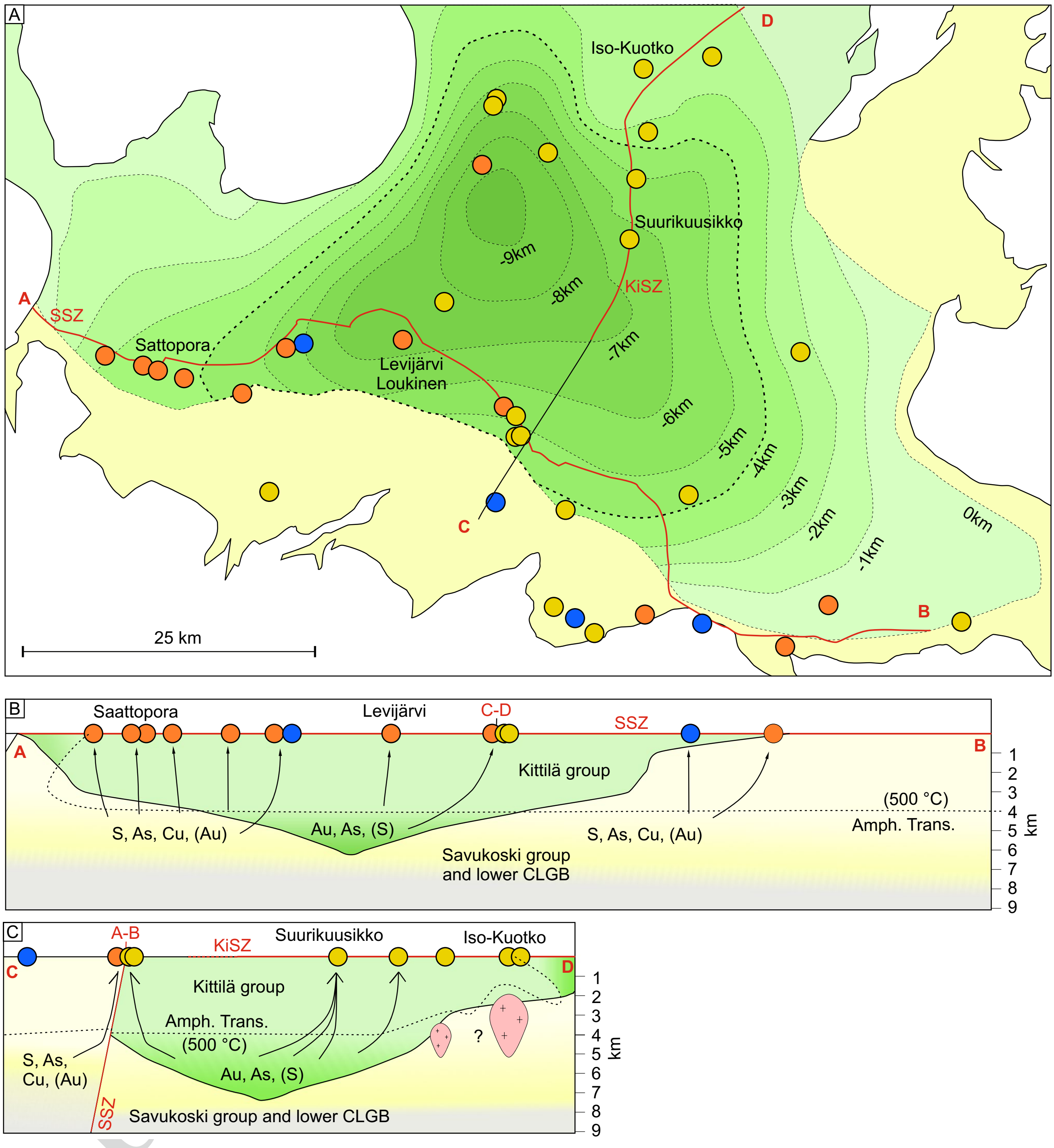

Fig. 10 Block model of the CLGB where metals are mobilized from the source at depth. **a** Projection of the Kittilä Group thickness from Niiranen et al. (2015) onto the surface. The greenschist to amphibolite facies transition occurs at > 4-km depth (thick dashed line). The typical deposits are located preferentially above the source dominated by the Kittilä Group whereas the atypical deposits are located preferentially above the Savukoski Group. **b** Schematic representation of the Sirkka shear zone (SiSZ) footwall with thickness of the Kittilä Group and potential metal source volumes. **c** Schematic representation of the Kiistala shear zone (KiSZ) prolonged to the SE with thickness of the Kittilä Group and potential metal source volumes. Ore deposit color legend as in Fig. 1

(29.7 vol%) implying that the metamorphic fluids would have been enriched in a larger suite of elements such as S, C, Cu, As, Se, Mo, Sn, Sb, Te, Au, and U (Table 6).

The lithological variability in the source is interpreted to have significant control on the style of mineralization and metal endowment in the orogenic Au deposits of the

Table 6 Mass balance calculations for metal mobilization from the source areas of the Kittilä and Savukoski groups

	S	C	Co	Cu	As	Se	Mo	Sn	Sb	Te	Au	U
	wt%	wt%	ppm	ppm	ppm	ppm	ppm	ppm	ppm	ppm	ppb	ppm
Protolith composition												
Kittilä Metavolcanic rocks	0.13	0.28	49.95	92.24	10.54	0.72	1.04	2.05	0.14	0.02	0.84	0.44
Kittilä Metasedimentary rocks	3.0	2.4	49.7	373.5	55.7	2.3	11.3	1.5	1.5	0.08	0.6	4.8
Savukoski Metavolcanic rocks	0.13	0.28	49.95	92.24	10.54	0.72	1.04	2.05	0.14	0.02	0.84	0.44
Savukoski Komatiites	0.08	1.32	93.70	4.24	0.85	0.15	0.05	0.12	0.19	0.01	0.43	0.03
Savukoski Metasedimentary rocks	3.0	2.4	49.7	373.5	55.7	2.3	11.3	1.5	1.5	0.1	0.6	4.8
Mass in source area (t)												
Kittilä Metavolcanic rocks	6.0E+09	1.3E+10	2.2E+08	4.1E+08	4.7E+07	3.2E+06	4.7E+06	9.2E+06	6.4E+05	9.3E+04	3.8E+03	2.0E+06
Kittilä Metasedimentary rocks	5.3E+08	4.1E+08	8.7E+05	6.6E+06	9.8E+05	4.1E+04	2.0E+05	2.6E+04	2.7E+04	1.5E+03	1.0E+01	8.5E+04
Savukoski Metavolcanic rocks	8.9E+08	1.9E+09	3.3E+07	6.2E+07	7.1E+06	4.8E+05	7.0E+05	1.4E+06	9.5E+04	1.4E+04	5.7E+02	3.0E+05
Savukoski Komatiites	7.7E+08	1.2E+10	8.5E+07	3.9E+06	7.8E+05	1.4E+05	4.5E+04	1.1E+05	1.8E+05	6.6E+03	4.0E+02	3.2E+04
Savukoski Metasedimentary rocks	2.0E+10	1.5E+10	3.2E+07	2.4E+08	3.6E+07	1.5E+06	7.4E+06	9.5E+05	9.9E+05	5.5E+04	3.7E+02	3.2E+06
Depletion (%)												
Kittilä Metavolcanic rocks	*−45.6*				−90.9			−71.5		−51.3	−58.7	
Kittilä Metasedimentary rocks	−92.9	−54.8		−70.9	−95.8	−66.7	−94.6	−62.7	−93.1	−89.1		−75.2
Savukoski Metavolcanic rocks	*−45.6*				−90.9			−71.5		−51.3	−58.7	
Savukoski Komatiites											*−87.0*	
Savukoski Metasedimentary rocks	−92.9	−54.8		−70.9	−95.8	−66.7	−94.6	−62.7	−93.1	−89.1		−75.2
Mass balance (t)												
Kittilä Metavolcanic rocks	*2.7E+09*				4.3E+07			6.6E+06		4.8E+04	2.2E+03	
Kittilä Metasedimentary rocks	4.9E+08	2.3E+08		4.7E+06	9.4E+05	2.7E+04	1.9E+05	1.6E+04	2.5E+04	1.3E+03		6.4E+04
Savukoski Metavolcanic rocks	*4.1E+08*				6.4E+06			9.8E+05		7.1E+03	3.3E+02	
Savukoski Komatiites											*3.4E+02*	
Savukoski Metasedimentary rocks	1.8E+10	8.4E+09		1.7E+08	3.5E+07	1.0E+06	7.0E+06	5.9E+05	9.2E+05	4.9E+04		2.4E+06
Total Kittilä	**4.9E+08**	**2.3E+08**		**4.7E+06**	**4.4E+07**	**2.7E+04**	**1.9E+05**	**6.6E+06**	**2.5E+04**	**4.9E+04**	**2.2E+03**	**6.4E+04**
Total Savukoski	**1.8E+10**	**8.4E+09**		**1.7E+08**	**4.1E+07**	**1.0E+06**	**7.0E+06**	**1.6E+06**	**9.2E+05**	**5.6E+04**	**6.8E+02**	**2.4E+06**
Total Kittilä and Savukoski	**1.9E+10**	**8.6E+09**		**1.8E+08**	**8.5E+07**	**1.0E+06**	**7.2E+06**	**8.2E+06**	**9.4E+05**	**1.1E+05**	**2.9E+03**	**2.4E+06**

Numbers in italic (S in metavolcanic rocks and Au in metakomatiites) have high uncertainties and are not included in the final mass balance calculations

Journal : Large 126 | Article No : 1133 | Pages : 28 | MS Code : 1133 | Dispatch : 10-9-2022

CLGB. The spatial distribution of the typical orogenic Au deposits along the KiSZ and SiSZ and the atypical along the SiSZ supports this argument. By projecting the thickness of the Kittilä Group onto the geological map, the dominant rock types present at depth in the source can be inferred (Fig. 10). Following the approach of Niiranen et al. (2015), the potential source is defined as the rock volume that has been metamorphosed at upper amphibolite-facies conditions (> 500–550 °C). In the Kittilä Group, the transition to amphibolite-facies conditions is inferred to be recorded at 4.05–5.35 km below the erosion surface level, based on greenschist-facies conditions recorded at the surface (~ 350 °C, Hölttä et al. 2007) and a temperature gradient of 37 °C/km during metamorphism (Niiranen et al. 2015). The transition to amphibolite facies becomes shallower in the CLGB to the north due to an inverted metamorphic gradient caused by thrusting of the Lapland Granulite Belt and to the west by thrusting of the Haparanda Suite (Fig. 10).

Although the block model in Fig. 10 only represents the end product of the Svecofennian orogeny, it still allows determination of the rock types potentially present in the source at the time of metamorphic evolution. The Kittilä Group is considered to prevail in the source volume where it is thicker than 4–5 km at depth, corresponding to the core of the CLGB, whereas the Savukoski Group prevails in the source volume where the Kittilä Group is thinner than 4–5 km and to the south of the SiSZ where the Kittilä Group is absent (Fig. 10). Along the KiSZ, the Kittilä Group is thick, especially in the southern section (> 7 km; Fig. 10), and thus, metamorphic fluids produced during metamorphic devolatilization of this rock volume would have been Au, As, and S-rich, accounting for the formation of typical orogenic Au deposit such as the Suurikuusikko deposit. The $\delta^{34}S$ signature of disseminated and vein-hosted auriferous pyrite in metavolcanic rocks at Suurikuusikko ranges between 0 and + 5‰ with few negative values for low Au bearing disseminated pyrite in metasedimentary rocks (to − 5‰; Molnár et al. 2017). The most common pyrite signature of 0 to + 5‰ can be attributed to a homogenized source, most likely buffered by the Kittilä Group metavolcanic rocks ($\delta^{34}S$ of altered oceanic crust of ~ + 1‰; Alt 1995; Molnár et al. 2017), whereas the few negative $\delta^{34}S$ values could be inherited from primary sedimentary-related pyrite or from fluids buffered by the Kittilä Group black schist (− 3 to + 4‰; Hanski and Huhma 2005).

The Kittilä Group present on the northern side of the SiSZ exceeds 4 km in thickness only over a limited area in the central part of the shear zone (Fig. 10). The Savukoski Group and possibly the other lower CLGB units and Archean basement are thus likely to be the dominant metal and ligand sources at depth along the SiSZ. Metamorphic fluid produced during metamorphic devolatilization would have been thus preferentially enriched in S, C, Cu, As, Se, Mo, Sn, Sb, Te, and U with lesser Au, promoting the formation of atypical orogenic Au along the SiSZ. The $\delta^{34}S$ signature of sulfides (pyrite, pyrrhotite, and chalcopyrite) from the Sattopora deposit ranges between 1 and + 4‰ in the northern orebody, in contact with the Kittilä Group and between − 1 and + 18‰ in the southern orebody, in contact with the Savukoski Group (Molnár et al. 2019). Within the wide range of the S isotope ratios in the southern orebody, two peaks are observed, one at ~ + 2‰ (range ~ − 1 to + 4‰), similarly to the northern orebody, and a second at ~ + 7– + 8‰ (range ~ + 5 to + 9‰; Molnár et al. 2019). The $\delta^{34}S$ range of sulfides form the northern and southern orebody between ~ − 1 and + 4‰ can be attributed to a source strongly buffered by metavolcanic rocks, similarly to the Suurikuusikko deposit (Molnár et al. 2019). Instead, the $\delta^{34}S$ range of sulfides from the southern orebody between ~ + 5 to + 9 ‰ is explained by buffering of the mineralizing fluids by the Savukoski Group black schists, which have high $\delta^{34}S$ values (up to + 27‰; Hanski and Huhma 2005; Molnár et al. 2019). The presence of light hydrocarbons in fluid inclusions from the Sattopora deposit may imply C-rich metasedimentary rocks in the source, such as Savukoski Group black schists (Molnár et al. 2019).

Metal mobilization and orogenic Au mineralization in an evolving orogen

Orogenic Au deposits in the CLGB show multiple hydrothermal events with distinct stages of ore accumulation (Wyche et al. 2015; Molnár et al. 2018; Sayab et al. 2019). Two main stages of orogenic Au mineralization are currently recognized within the CLGB defined by an early-stage associated with peak metamorphism and a stage associated with late orogenic evolution (e.g., Molnár et al. 2018). The relationship between metal source zones and ore deposits is, however, difficult to establish as the ages of the causative metamorphic events for metal mobilization from the different units of the CLGB, mainly the Kittilä and Savukoski groups, are poorly constrained.

1. Au mineralization related to peak metamorphism

The earliest known mineralizing stage occurred within the Kittilä Group along the KiSZ and is defined by the main Au stage of the Suurikuusikko deposit, which is dated at 1.916 Ga and interpreted to be related to D1 (Wyche et al. 2015; Sayab et al. 2019). Prograde metamorphic devolatilization of rocks belonging to the Kittilä Group (Fig. 10) is interpreted to have occurred close to peak metamorphism at ~ 1.88–1.86 Ga, related to D2–D3 and generating Au-, As-, and S-rich metamorphic fluids. A conundrum arises as the Re-Os isochron age of the Suurikuusikko deposit (1.916 ± 0.016 Ga) pre-dates peak metamorphism and associated metal mobilization. This discrepancy is difficult to account for, but further dating of both the Surrikuusiko deposit and peak metamorphism of the Kittilä and Savukoski groups could provide new insight. For instance, the northern part of the CLGB, in addition to inverted metamorphism, has been intruded by various magmatic bodies such as the Taatsi granodiorite (1.92–1.91 Ga), the Ruoppapalo granodiorite (1.91–1.90 Ga; Nironen 2017), and numerous porphyry dikes within the Kittilä Group dated at ca. 1.92 Ga (Rastas et al. 2001; Molnár et al. 2018). The effect of numerous magmas intruding or underplating the Kittilä Group could have led to substantial heating at its base, especially in its north-northeastern part. The combined effect of inverted metamorphic gradient, due to thrusting of the Lapland Granulite Belt, and the excessive external heat from magmatic bodies possibly led to earlier peak metamorphism and metamorphic devolatilization at the base of Kittilä Group than in its shallower part, resembling to a "deep-earlier" metamorphic scenario (Stüwe et al. 1993; Stüwe 1998). Apart from the Suurikuusikko age conundrum, the Iso-Kuotko minimum age of mineralization at 1.87–1.86 Ga and associated with D1–D3 (Molnár et al. 2018; Sayab et al. 2019) fits with metal mobilization from the Kittilä Group source zone during prograde metamorphic devolatilization. Noteworthy, stress regime switch from compression (D2, ~ 1.90–1.89 Ga) to transpression (D3, ~ 1.88–1.87 Ga) would have increased crustal permeability, favoring large-scale fluid migration along major shear zone (e.g., KiSZ) and ore formation (Goldfarb et al. 1991, 2005; Bierlein et al. 2004; Sayab et al. 2019).

2. Au mineralization during late orogenic evolution

The second major epigenetic-hydrothermal typical and atypical stage that occurred in the CLGB during the latest stages of the Svecofennian orogeny corresponds to the main mineralization stages in the Iso-Kuotko, Saattopora and Levijärvi deposits (Patison 2007; Molnár et al. 2018, 2019; Sayab et al. 2019). These stages, occurring within a time window from ca. 1.83 to 1.76 Ga, are associated with D4–D5 deformation (Patison 2007; Molnár et al. 2018; Sayab et al. 2019) and appear apparently incompatible with metal mobilization during prograde metamorphic devolatilization during D2–D3. During the late Svecofennian orogeny evolution, however, a widespread thermal event, granitoid magmatism and high-grade metamorphism occurred (Hölttä et al. 2020), such as in the eastern Pajala Shear Zone (ca. 1.82–1.78 Ga; Bergman et al. 2006), the Hetta Complex (ca. 1.77 Ga; Ahtonen et al. 2007), and in parts of the Central Lapland Granitoid Complex (1.90–1.76 Ga; Corfu and Evins 2002; Nironen 2017; Lahtinen et al. 2018). The causes of this magmatism and metamorphism, such as lithospheric delamination, crustal erosion and asthenospheric upwelling, crustal melting following orogenic thickening or the far field effect of the amalgamation of Amazonia, Sarmatia, and Svecofennia (Corfu and Evins 2002; Lahtinen et al. 2005; Kukkonen et al. 2008), remain cryptic but most likely resulted in regional-scale lithospheric heating of the crust (Hölttä et al. 2020). Such event could have led to late-stage metamorphic fluid flow (Gonçalves et al. 2019), likely during D4–D5 (~ 1.84–1.76 Ga), associated with the SiSZ reactivation (Patison 2007) and possibly with late-stage metal mobilization from rocks that might have sustained only limited metal loss during earlier metamorphic devolatilization events. Again, a better understanding of the metamorphic evolution of the group units throughout the CLGB, especially of the Savukoski Group south of the SiSZ, would allow to build more robust genetic links between metal mobilization from source zones and ore deposits. Alternatively to metamorphic devolatilization, deep crustal or subcontinental lithospheric mantle fluid could have been generated during the latest stages of orogenic evolution accounting for the late-stage mineralizing events in the CLGB (Goldfarb and Groves 2015). A deep crustal source of mineralizing fluids is suggested by the Pb isotopic signature of galena from the Iso-Kuotko deposit, which shows an Archean basement component (Molnár et al. 2018). However, the different metal endowment of deposits along the KiSZ and SiSZ still suggests partial control of a shallower crustal source possibly explained by mixing of deep and mid-crustal fluids (LaFlamme et al. 2018).

Conclusions

Characterization of metal mobilization during prograde metamorphism of metavolcanic rocks, metasedimentary rocks, and metakomatiite from the CLGB enables us to test the metamorphic devolatilization model applied to the Paleoproterozoic greenstone belt. The main outcomes of the study are:

- The different investigated rock types show different metal mobilization during prograde metamorphism. Metavolcanic rocks show strong Au, As, and Sn and also possibly S depletion. Sulfur- and C-rich (S + C > 1 wt%) metasedimentary rocks show significant depletion of S, C, Cu, As, Se, Mo, Sn, Sb, Te, and U. Limited data from metakomatiite suggest that Au could be mobilized during prograde metamorphism. No clear mobilization of Ni and Co has been related to metamorphic devolatilization.
- When investigating metamorphic devolatilization from a source, all the rock types present should be considered and not only the dominant one. The metamorphic fluids produced from the devolatilization of the Kittilä Group were preferentially enriched in Au, As, Sn, Te, and S with the metavolcanic rocks (> 95% vol.) providing the bulk of these elements. The minor metasedimen-

Journal : Large 126	Article No : 1133	Pages : 28	MS Code : 1133	Dispatch : 10-9-2022

tary rocks (< 5% vol.) most likely acted as an additional source, enhancing the metamorphic fluid metal content. On the contrary, metamorphic devolatilization from the Savukoski Group led to metamorphic fluids preferentially enriched in S, C, Cu, As, Se, Mo, Sn, Sb, Te, and U due to the large volume of metasedimentary rocks (> 40% vol.). These metamorphic fluids possibly had limited Au enrichment, relative to the Kittilä Group, due to the lower volume of metavolcanic rocks (~ 34% vol.) and the lack of Au depletion from the metasedimentary rocks.

- The style of mineralization and the bulk metal endowment of the deposits are strongly controlled by the nature of the source rocks at depth. Block reconstruction of the central CLGB highlights that the source of typical orogenic Au deposits along the KiSZ is dominated at depth by the Kittilä Group whereas the source of atypical Au deposits along the SiSZ is dominated at depth by the Savukoksi Group.
- A two stage model for Au mineralization in the CLGB is proposed:

  1. The primary stage associated with metamorphic devolatilization related to early stage of prograde metamorphism reaching peak metamorphism at ~ 1.88–1.86 Ga related to D2–D3. Devolatilization occurred preferentially from the Kititilä Group promoting the formation of typical orogenic Au deposits. Better dating of the metamorphic evolution of the CLGB unit groups, especially in the northern part of the belt, could reveal if this process can account for the formation of the Suurikuusikko deposit which predates peak metamorphism according to the presently available geochronological data. This stage occurred mainly within the Kittilä Group and along the KiSZ.
  2. The second stage associated with late orogenic evolution between ~ 1.83 and 1.76 Ga. In addition to the typical orogenic gold deposits, gold ores with atypical metal associations were also formed. Widespread granitoid magmatism, indicating that the mid-crust was at least locally hot at this stage of tectonic evolution, and high-grade metamorphism present throughout the Svecofennian orogeny, likely promoted late metamorphic fluid flow and possibly late metal mobilization. Additionally, deep crustal fluids from the lower crust or even the sub-continental lithospheric mantle could have been involved. This stage is mainly recorded along the SiSZ.

Within the frame of the debate regarding the source of metals in orogenic Au deposit, this study highlights that in the CLGB, and most likely in other Precambrian greenstone belts, combined metamorphic devolatilization of both metavolcanic and metasedimentary rocks can account for the formation of orogenic Au deposits. Further insight, however, could be gained by better linking the causative metamorphic events responsible for metal mobilization from the source zones with the ore deposits throughout the complex tectono-metamorphic evolution of an orogeny. Finally, mobilization of metals by metamorphic devolatilization does not preclude the implication of other deep-seated or magmatic sources which might also contribute also to orogenic Au endowment of Precambrian greenstone belts.

Supplementary Information The online version contains supplementary material available at https://doi.org/10.1007/s00126-022-01133-z.

Acknowledgements The authors would like to thank R. Goldfarb and an anonymous reviewer for thorough reviews as well as H. Frimmel and G. Beaudoin for editorial handling.

Funding Open Access funding enabled and organized by Projekt DEAL. This research was financially supported the Academy of Finland supported MinSysPro – Mineral Systems and Mineral Prospectivity in Finnish Lapland (grant No.281670) and the Academy of Finland and DAAD supported OroTecT (Orogenic gold deposits and post-orogenic tectonothermal evolution on Precambrian terranes: sources of ore-forming components and preservation of ore deposist – grant no. 315188) projects. Partial financial support was provided by Stockholm University, Sweden.

Declarations

Conflict of interest The authors declare no competing interests.

References

Ahtonen N, Holtta P, Huhma H (2007) Intracratonic Palaeoproterozoic granitoids in northern Finland: prolonged and episodic crustal melting events revealed by Nd isotopes and U-Pb ages on zircon. Bull Geol Soc Finl 79:143

Alt JC (1995) Sulfur isotopic profile through the oceanic crust: sulfur mobility and seawater-crustal sulfur exchange during hydrothermal alteration. Geology 23:585–588

Augustin J, Gaboury D (2017) Plume-related basaltic rocks in the Mana gold district in western Burkina Faso, West Africa : implications for exploration and the source of gold in orogenic deposits. J Afr Earth Sci Paleoproterozoic 129:17–30

Barnes S-J, Often M (1990) Ti-rich komatiites from northern Norway. Contrib to Mineral Petrol 105:42–54

Beaudoin G, Chiaradia M (2016) Fluid mixing in orogenic gold deposits: evidence from the HO-Sr isotope composition of the Val-d'Or vein field (Abitibi, Canada). Chem Geol 437:7–18

Bergman S, Billström K, Persson P-O et al (2006) U-Pb age evidence for repeated Palaeoproterozoic metamorphism and deformation near the Pajala shear zone in the northern Fennoscandian shield. GFF 128:7–20

Bhatia MR, Crook KAW (1986) Trace element characteristics of greywackes and tectonic setting discrimination of sedimentary basins. Contrib Mineral Petrol 92:181–193

Bierlein FP, Christie AB, Smith PK (2004) A comparison of orogenic gold mineralisation in central Victoria (AUS), western South Island (NZ) and Nova Scotia (CAN): implications for variations in the endowment of Palaeozoic metamorphic terrains. Ore Geol Rev 25:125–168

Boyle RW (1966) Origin of the gold and silver in the gold deposits of the Meguma Series. Nova Scotia Can Mineral 8:662

Brugger J, Liu W, Etschmann B et al (2016) A review of the coordination chemistry of hydrothermal systems, or do coordination changes make ore deposits? Chem Geol 447:219–253

Burrows DR, Wood PC, Spooner ETC (1986) Carbon isotope evidence for a magmatic origin for Archaean gold-quartz vein ore deposits. Nature 321:851

Corfu F, Evins PM (2002) Late Palaeoproterozoic monazite and titanite U-Pb ages in the Archaean Suomujärvi Complex, N-Finland. Precambrian Res 116:171–181

Crocket JH (1993) Distribution of gold in the Earth' s crust. In: Foster RP (eds) Gold Metallogeny and Exploration, vol 1, p 36

de Wit MJ, Ashwal LD (1995) Greenstone belts: what are they? South African J Geol 98:505–520

Eilu P, Pankka H, Keinänen V et al (2007) Characteristics of gold mineralisation in the greenstone belts of northern Finland. Geol Surv Finland Spec Pap 44:57–106

Eilu P (2015) Overview on gold deposits in Finland. In: Maier WD, Lahtinen R, O'Brien H (eds) Mineral deposits of Finland. Elsevier, Amsterdam, pp 377–410

Frietsch R, Tuisku P, Martinsson O, Perdahl J-A (1997) Early proterozoic Cu-(Au) and Fe ore deposits associated with regional Na-Cl metasomatism in northern Fennoscandia. Ore Geol Rev 12:1–34

Frimmel HE (2018) Episodic concentration of gold to ore grade through Earth's history. Earth-Sci Rev 180:148–158

Fyfe WS (1987) Tectonics, fluids and ore deposits: mobilization and remobilization. Ore Geol Rev 2:21–36

Gaboury D (2019) Parameters for the formation of orogenic gold deposits. Appl Earth Sci 128:124–133

Goldfarb RJ, Groves DI (2015) Orogenic gold: common or evolving fluid and metal sources through time. Lithos 233:2–26

Goldfarb RJ, Snee LW, Miller LD, Newberry RJ (1991) Rapid dewatering of the crust deduced from ages of mesothermal gold deposits. Nature 354:296–298

Goldfarb R, Baker T, Dube B et al (2005) Distribution, character and genesis of gold deposits in metamorphic terranes. Econ Geol 100th Anniv Vol 407–450

Gonçalves GO, Lana C, Buick IS et al (2019) Twenty million years of post-orogenic fluid production and hydrothermal mineralization across the external Araçuaí orogen and adjacent São Francisco craton, SE Brazil. Lithos 342:557–572

Groves DI (1993) The crustal continuum model for late-Archaean lode-gold deposits of the Yilgarn Block, Western Australia. Miner Depos 28:366–374

Groves DI, Phillips GN (1987) The genesis and tectonic control on Archaean gold deposits of the western Australian shield—a metamorphic replacement model. Ore Geol Rev 2:287–322

Groves DI, Goldfarb RJ, Gebre-Mariam M et al (1998) Orogenic gold deposits: a proposed classification in the context of their crustal distribution and relationship to other gold deposit types. Ore Geol Rev 13:7–27

Groves DI, Santosh M, Deng J et al (2019) A holistic model for the origin of orogenic gold deposits and its implications for exploration. Miner Depos 55:1–18

Groves DI (1998) Orogenic gold deposits: a proposed classification in the context of their crustal distribution and relationship to other gold deposit types

Hanski E, Huhma H, Rastas P, Kamenetsky VS (2001a) The Palaeoproterozoic komatiite–picrite association of Finnish Lapland. J Petrol 42:855–876

Hanski E, Huhma H, Vaasjoki M (2001b) Geochronology of northern Finland : a summary and discussion. Geol Surv Finl Spec Pap 33:255–279

Hanski E, Huhma H (2005) Central Lapland greenstone belt. In: Lehtinen M, Nurmi PA, Rämö OT (eds) Precambrian Geology of Finland - Key to the Evolution of the Fennoscandian Shield. Elesvier B. V., pp 139–194

Heggie GJ, Barnes SJ, Fiorentini ML (2013) Application of lithogeochemistry in the assessment of nickel-sulphide potential in komatiite belts from northern Finland and Norway. Bull Geol Soc Finl 85:107–126

Herron MM (1988) Geochemical classification of terrigenous sands and shales from core or log data. J Sediment Res 58:820–829

Holma MJ, Keinanen VJ (2007) The Levijärvi–Loukinen gold occurrence: an example of orogenic gold mineralization with atypical metal association. In: Ojala VJ (eds) Goldin the Central Lapland Greenstone Belt, Finland. Geol Surv Finl Spec Pap, pp 165–184

Hölttä P, Heilimo E (2017) Metamorphic map of Finland. Geol Surv Finland Spec Pap 60:77–128

Hölttä P, Väisänen M, Väänänen J, Manninen T (2007) Paleoproterozoic metamorphism and deformation in Central Lapland, Finland. Gold Cent Lapl Greenstone Belt Geol Surv Finl Spec Pap 44:9–58

Hölttä P, Huhma H, Lahaye Y et al (2020) Paleoproterozoic metamorphism in the northern Fennoscandian Shield: age constraints revealed by monazite. Int Geol Rev 62:360–387

Hronsky JMA, Groves DI, Loucks RR, Begg GC (2012) A unified model for gold mineralisation in accretionary orogens and implications for regional-scale exploration targeting methods. Miner Depos 47:339–358

Hu S-Y, Evans K, Fisher L et al (2016) Associations between sulfides, carbonaceous material, gold and other trace elements in polyframboids: implications for the source of orogenic gold deposits, Otago Schist, New Zealand. Geochim Cosmochim Acta 180:197–213

Jenner FE, O'Neill HSC (2012) Major and trace analysis of basaltic glasses by laser-ablation ICP-MS. Geochem Geophys Geosystems 13:1–17

Jochum KP, Verma SP (1996) Extreme enrichment of Sb, Tl and other trace elements in altered MORB. Chem Geol 130:289–299. https://doi.org/10.1016/0009-2541(96)00014-9

Jowitt SM, Jenkin GRT, Coogan LA, Naden J (2012) Quantifying the release of base metals from source rocks for volcanogenic massive sulfide deposits: effects of protolith composition and alteration mineralogy. J Geochem Explor 118:47–59

Ketris MP, Yudovich YE (2009) Estimations of Clarkes for Carbonaceous biolithes: world averages for trace element contents in black shales and coals. Int J Coal Geol 78:135–148

Kolb J, Dziggel A, Bagas L (2015) Hypozonal lode gold deposits : a genetic concept based on a review of the New Consort, Renco, Hutti, Hira Buddini, Navachab, Nevoria and The Granites deposits. Precambrian Res 262:20–44

Kukkonen IT, Kuusisto M, Lehtonen M, Peltonen P (2008) Delamination of eclogitized lower crust: control on the

crust–mantle boundary in the central Fennoscandian shield. Tectonophysics 457:111–127
Kurhila M, Molnár F, O'Brien H et al (2017) U-Pb dating of hydrothermal monazite and xenotime from the Levijärvi-Loukinen gold deposit, Central Lapland Greenstone Belt, Northern Finland. In: 3rd Finnish National Colloquium of Geosciences Espoo, 15–16 March 2017. p 56
LaFlamme C, Jamieson JW, Fiorentini ML et al (2018) Investigating sulfur pathways through the lithosphere by tracing mass independent fractionation of sulfur to the Lady Bountiful orogenic gold deposit, Yilgarn Craton. Gondwana Res 58:27–38
Lahtinen R, Huhma H, Sayab M et al (2018) Age and structural constraints on the tectonic evolution of the Paleoproterozoic Central Lapland Granitoid Complex in the Fennoscandian Shield. Tectonophysics 745:305–325
Lahtinen R, Korja A, Nironen M (2005) Paleoproterozoic tectonic evolution. In: Developments in Precambrian Geology. Elsevier, pp 481–531
Large RR, Bull SW, Maslennikov VV (2011) A carbonaceous sedimentary source-rock model for Carlin-type and orogenic gold deposits. Econ Geol 106:331–358
Large RR, Halpin JA, Danyushevsky LV et al (2014) Trace element content of sedimentary pyrite as a new proxy for deep-time ocean–atmosphere evolution. Earth Planet Sci Lett 389:209–220
Large RR, Gregory DD, Steadman JA et al (2015) Gold in the oceans through time. Earth Planet Sci Lett 428:139–150
Le Bas MJ (2000) IUGS Reclassification of the high-Mg and picritic volcanic rocks. J Petrol 41:1467–1470
Le Bas MJ, Le Maitre RW, Streckeisen A et al (1986) A chemical classification of volcanic rocks based on the total alkali-silica diagram. J Petrol 27:745–750
Lehtonen M, Airo ML, Eilu P et al (1998) The stratigraphy, petrology and geochemistry of the Kittilä greenstone area, northern Finland. A Report of the Lapland Volcanite Project. Geol Surv Finland, Rep Investig 140:1–144
Masurel Q, Thébaud N, Allibone A et al (2019) Intrusion-related affinity and orogenic gold overprint at the Paleoproterozoic Bonikro Au–(Mo) deposit (Côte d'Ivoire, West African Craton). Miner Depos 57:557–580
McCuaig TC, Kerrich R (1998) P—T—t—deformation—fluid characteristics of lode gold deposits: evidence from alteration systematics. Ore Geol Rev 12:381–453
McDonough WF, Sun Ss (1995) The composition of the Earth. Chem Geol 120:223–253
Mineral Deposit Database of Finland (2022) Digital map database [Electronic resource]. Geological Survey of Finland [referred 21.01.2022]. Available at: http://gtkdata.gtk.fi/MDaE/index.html
Molnár F, Middleton A, Stein H et al (2018) Repeated syn-and post-orogenic gold mineralization events between 1.92 and 1.76 Ga along the Kiistala Shear Zone in the Central Lapland Greenstone Belt, northern Finland. Ore Geol Rev 101:936–959
Molnár F, Lahaye Y, Hugh Ob et al (2019) The Saattopora orogenic Au-Cu deposit, Central Lapland Greenstone belt, Finland: fluid sources and timing of hydrothermal processes. In: 15th Biennal SGA Meeting. pp 723–726
Molnár F, OBrien H, Lahaye Y et al (2017) Multi-stage hydrothermal processes and diverse metal associations in orogenic gold deposits of the Central Lapland Greenstone Belt, Finland. In: Mineral Resources to Discover–14th SGA Biennial Meeting. pp 63–66
Nesbitt BE, St. Louis RM, Muehlenbachs K (1987) Distribution of gold in altered basalts of DSDP hole 504B. Can J Earth Sci 24:201–209
Niiranen T, Lahti I, Nykänen V (2015) The orogenic gold potential of the Central Lapland Greenstone Belt, Northern Fennoscandian Shield. In: Mineral Deposits of Finland. Elsevier, pp 733–752
Nironen M (2017) Structural interpretation of the Peräpohja and Kuusamo belts and Central Lapland, and a tectonic model for northern Finland. Geol Surv Finland Rep Investig 234:53
Patison NL (2007) Structural controls on gold mineralisation in the Central Lapland Greenstone Belt. In: Gold in the Central Lapland Greenstone Belt, Finland, pp 107–122
Patten CGC, Pitcairn IK, Teagle DAH, Harris M (2016) Mobility of Au and related elements during the hydrothermal alteration of the oceanic crust: implications for the sources of metals in VMS deposits. Miner Depos 51:179–200
Patten CGC, Pitcairn IK, Molnár F et al (2020) Gold mobilization during metamorphic devolatilization of Archean and Paleoproterozoic metavolcanic rocks. Geology 48:1110–1114
Pearce JA, Norry MJ (1979) Petrogenetic implications of Ti, Zr, Y, and Nb variations in volcanic rocks. Contrib Mineral Petrol 69:33–47
Phillips GN, Powell R (2010) Formation of gold deposits: a metamorphic devolatilization model. J Metamorph Geol 28:689–718
Phillips GN, Groves DI, Brown IJ (1987) Source requirements for the Golden Mile, Kalgoorlie: significance to the metamorphic replacement model for Archean gold deposits. Can J Earth Sci 24:1643–1651
Pitcairn IK (2011) Background concentrations of gold in different rock types. Appl Earth Sci 120:31–38
Pitcairn IK, Teagle DAH, Craw D et al (2006a) Sources of metals and fluids in orogenic gold deposits: insights from the Otago and Alpone schists, New Zealand. Econ Geol 101:1525–1546
Pitcairn IK, Warwick PE, Milton JA, Teagle DAH (2006b) Method for ultra-low-level analysis of gold in rocks. Anal Chem 78:1290–1295
Pitcairn IK, Craw D, Teagle DAH (2015) Metabasalts as sources of metals in orogenic gold deposits. Miner Depos 50:373–390
Pitcairn IK, Leventis N, Beaudoin G et al (2021) A metasedimentary source of gold in Archean orogenic gold deposits. Geology 49:862–866
Qiu Z-J, Fan H-R, Goldfarb R et al (2021) Cobalt concentration in a sulfidic sea and mobilization during orogenesis: implications for targeting epigenetic sediment-hosted Cu-Co deposits. Geochim Cosmochim Acta 305:1–18
Rastas P, Huhma H, Hanski E et al (2001) U-Pb isotopic studies on the Kittila greenstone area, central Lapland, Finland. Geol Surv Finland Spec Pap 33:95–142
Ross P-S, Bédard JH (2009) Magmatic affinity of modern and ancient subalkaline volcanic rocks determined from trace-element discriminant diagrams. Can J Earth Sci 46:823–839
Sayab M, Suuronen J-P, Molnár F et al (2016) Three-dimensional textural and quantitative analyses of orogenic gold at the nanoscale. Geology 44:739–742
Sayab M, Molnár F, Aerden D et al (2019) A succession of near-orthogonal horizontal tectonic shortenings in the Paleoproterozoic Central Lapland Greenstone Belt of Fennoscandia: constraints from the world-class Suurikuusikko gold deposit. Miner Depos 55:1605–1624
Schandl ES, Gorton MP (2012) Hydrothermal alteration and CO2 metasomatism (natural carbon sequestration) of komatiites in the south-western Abitibi greenstone belt. Can Mineral 50:129–146
Stüwe K (1998) Tectonic constraints on the timing relationships of metamorphism, fluid production and gold-bearing quartz vein emplacement. Ore Geol Rev 13:219–228
Stüwe K, Will TM, Zhou S (1993) On the timing relationship between fluid production and metamorphism in metamorphic piles: some implications for the origin of post-metamorphic gold mineralisation. Earth Planet Sci Lett 114:417–430

Journal : Large 126	Article No : 1133	Pages : 28	MS Code : 1133	Dispatch : 10-9-2022

Tatsumi Y, Oguri K, Shimoda G (1999) The behaviour of platinum-group elements during magmatic differentiation in Hawaiian tholeiites. Geochem J 33:237–247

Thébaud N, Sugiono D, LaFlamme C et al (2018) Protracted and polyphased gold mineralisation in the Agnew district (Yilgarn Craton, Western Australia). Precambrian Res 310:291–304

Tomkins AG (2010) Windows of metamorphic sulfur liberation in the crust : implications for gold deposit genesis. Geochim Cosmochim Acta 74:3246–3259

Vasilopoulos M, Molnár F, O'Brien H et al (2021) Geochemical signatures of mineralizing events in the Juomasuo Au–Co deposit, Kuusamo belt, northeastern Finland. Miner Depos 56:1195–1222

Webber AP, Roberts S, Taylor RN, Pitcairn IK (2013) Golden plumes: substantial gold enrichment of oceanic crust during ridge-plume interaction. Geology 41:87–90

Wyche NL, Eilu P, Koppström K et al (2015) The Suurikuusikko gold deposit (Kittilä mine), northern Finland. In: Mineral deposits of Finland. Elsevier, pp 411–433

Wyman D, Kerrich R (1988) Alkaline magmatism, major structures, and gold deposits; implications for greenstone belt gold metallogeny. Econ Geol 83:454–461

Publisher's note Springer Nature remains neutral with regard to jurisdictional claims in published maps and institutional affiliations.

Journal : Large 126 | Article No : 1133 | Pages : 28 | MS Code : 1133 | Dispatch : 10-9-2022